SYSTEMATIC CONTROL OF SCHOTTKY BARRIER HEIGHT

BY PARTISAN INTERLAYERS

by

Yang Li

A dissertation submitted to the Graduate Faculty in Physics in partial fulfillment of the requirements for the degree of Doctor of Philosophy,

The City University of New York

2012

© 2012

Yang Li

All Rights Reserved

This manuscript has been read and accepted for the
Graduate Faculty in Physics in satisfaction of the
dissertation requirement for the degree of Doctor of Philosophy.

Raymond T. Tung

______________ ______________________________
Date Chair of Examining Committee

Steven G. Greenbaum

______________ ______________________________
Date Executive Officer

Robert A. Bartynski

Nicolas Giovambattista

Mim Lal Nakarmi

Yuhang Ren

Supervisory Committee

THE CITY UNIVERSITY OF NEW YORK

ABSTRACT

Systematic Control of Schottky Barrier Height by Partisan Interlayer

by

Yang Li

Advisor: Professor Raymond T. Tung

The relationship between the starting surface structure and the Schottky barrier height (SBH) in metal-silicon systems has been investigated to explore the possibility of modifying the interface dipole through the insertion of an inorganic interface layer. A systematic and comprehensible way to perform this modification has been introduced as a "partisan interlayer" method and was extensively studied for a variety of interlayer elements, along with several choices for the metal. Employing elements with a larger electronegativity than that of silicon, a monolayer of As, S, or Cl was deposited on Si surfaces and processed to form stable surface structures. The electron affinities of these surfaces were measured by Kelvin probe and found to increase significantly from the clean surface, consistent with the expected charge transfer from Si to the adsorbates and also in agreement with results of ab initio density functional theory calculations. Subsequent deposition of metal on these adsorbate terminated semiconductor (ATS) surfaces led to the fabrication of metastable interface structures with the SBH successfully and significantly modified in a predictable manner from the clean Si results. The chemical stability of these surfaces that weakens the interaction with the deposited metal, likely leads to the preservation of electric dipole from such partisan interlayers. The partisan interlayer method was found to work particularly well with As-terminated Si(111) surface, on which a interface

behavior parameter exceeding 0.50 was found. This exceeded the S-parameter usually observed for covalent semiconductors such as Si, ~ 0.1, and highlighted a major reason for the adjustability of the SBH by the PI method. The SBH of all interfaces studied in this work was inhomogeneous. Making use of the theory of electronic transport through inhomogeneous SBH and temperature-dependent measurements, the extent of the SBH nonuniformity was routinely characterized from the Schottky diodes. The largest adjustment in the SBH was observed for Au on S-terminated Si(100), where the n-type junction became nearly perfectly ohmic. It was demonstrated, for the first time, that quantitative information on the distribution of the SBH and the lateral size of conduction patches ("hot spots") could still be obtained from ohmic junctions. The physical basis for these analyses and the special experimental conditions which enabled these analyses were carefully explained. The implications of these results for SBH control of MS systems in general and the understanding of the formation of SBH in general are also discussed.

TABLE OF CONTENTS

ABSTRACT iv

CHAPTER 1. Introduction 1

1.1 Schottky Barrier Height 2

1.2 Interface Dipole 4

1.3 Main Idea behind This Thesis 7

CHAPTER 2. Background 8

2.1 Partisan Interlayer 8

2.2 Adsorbate-Terminated Surfaces 11

2.3 Metal 15

CHAPTER 3. Experiment 16

3.1 UHV Chamber 17

3.1.1 Shadow Mask Mounting 18

3.1.2 Isolated Fabrication Vessel 19

3.1.3 Sample Transfer Mechanism 20

3.1.4 Glass Reactor 21

3.2 Experimental Procedures 22

3.3 Surface Characterization 25

3.4 Electrical Measurement 26

CHAPTER 4. Electron Affinity of Adsorbate-Terminated Silicon Surfaces 28

CHAPTER 5. Controlled Modification of Schottky Barrier Height by Partisan Interlayer between Ag and Si(111) 31

CHAPTER 6. Schottky Barriers on S-Terminated Si(100): Ohmic Contact without Heavy Doping! 39

CHAPTER 7. Effect of Metal Interaction on the Schottky Barrier Height on the Adsorbate-Terminated Si Surfaces 55

CHAPTER 8. Summary 64

APPENDIX 65

A. Camel Doping 65

B. Ohmic Analysis 67

REFERENCES 70

LIST OF TABLES

Table I. Ab initio DFT calculations in the slab geometry.. 14

Table II. Work function/electron affinity of adsorbate-terminated Si. 29

Table III. SBH of Ag on adsobate-terminated Si(111). 36

Table IV. Summary of SBHs of In, Ag and Au on S-terminated Si(100) surfaces, measured by I-V (Φ_{I-V}), C-V (Φ_{C-V}), and activation energy (Φ_{AE}) techniques. I-V, AE results and ideality factors are presented as a range. 46

Table V. Summary of SBHs of In, Ag and Au on clean, As-, S- and Cl-terminated Si surfaces, measured by I-V (Φ_{I-V}), C-V (Φ_{C-V}), and activation energy (Φ_{AE}) techniques. I-V, AE results and ideality factors are presented as a range. 58

Table VI. Summary of C-V measured n-type SBHs of In, Ag, and Au on clean and ATS surfaces. (*The n-type Au/Si(100)1×1-S SBH value was the Si band gap minus p-type SBH.) 60

LIST OF FIGURES

Figure 1. First order Schottky-Mott model of metal-semiconductor contacts. 3

Figure 2. Schematic of interface dipole. 5

Figure 3. Schematic representations of atomic layers making up metal (M) – interlayer (I) – semiconductor (S) interfaces and the formation of interface dipole. 8

Figure 4. Atomic structures of adorbate-teminated silicon surfaces. 12

Figure 5. A picture of the dual-station ultra-high vacuum chamber constructed for the present experimental work. 16

Figure 6. Structural view of main components installed in the UHV system. 17

Figure 7. Shadow mask mounting mechanism. 18

Figure 8. Isolation settings for the fabrication station. 19

Figure 9. Sample transfer and pick-up mechanism. 20

Figure 10. Glass reaction system for the gaseous-phase Cl-termination process. 21

Figure 11. Representative LEED patterns. 25

Figure 12. Kelvin Probe measurement of work function change by Cl-termination on Si(111).. 29

Figure 13. Kelvin Probe measurements of work function change by (a) As-termination on Si(111), (b) S-termination on Si(100), and (c) H-termination on Si(111). 30

Figure 14. Experimental I-V curves, obtained at 175 K, for Schottky diodes fabricated on clean, H-, As- and Cl-terminated Si (111) surfaces: (a) n-type (b) p-type. 32

Figure 15. Representative I-V curves under forward bias from Schottky diodes of Ag on (a) clean, (b) H-terminated, (c) As-terminated and (d) Cl-terminated Si(111) surfaces, showing ideality factors at each individual temperature. 33

Figure 16. Richardson plots for the Schottky junctions of Ag on clean and various adsorbate-terminated Si(111) substrates, (a) n-type, (b) p-type. 34

Figure 17. Experimental C-V characteristics for Schottky diodes formed on clean, H-, As- and Cl-terminated Si (111) surfaces, (a) n-type, (b) p-type. 35

Figure 18. I-V characteristics at various temperatures for Ag Schottky barriers on Si(100). 42

Figure 19. Representative I-V curves under forward bias from Schottky diodes of Au on (a) clean Si(100)2×1 and (b) S-terminated Si(100)1×1 surfaces, both p-type, showing ideality factors and SBH at each individual temperature. 43

Figure 20. Experimental C-V characteristics for Schottky diodes of Ag formed on clean and S-terminated Si(100) surfaces. 44

Figure 21. Richardson's plots of the saturation currents of Ag Schottky barriers formed on clean and S-terminated Si(100) surfaces. 45

Figure 22. IV characteristics from experiment and numerical simulation. 48

Figure 23. Possible components of small patches contributing to the ohmic behavior of n-type Si(100)1×1-S-Au. 51

Figure 24. I-V characteristics from two additional diodes on the Au/n-Si(100)1×1-S samples... 53

Figure 25. I-V characteristics at various temperatures for Au Schottky barriers on Si(111). 56

Figure 26. Representative C-V characteristics for Schottky diodes of (a) Au and (b) In formed on p-type clean, As and Cl-terminated Si(111) surfaces. 57

Figure 27. Dependence of n-type Schottky barrier heights on metal work function. 61

CHAPTER 1. Introduction

As modern electronic and optoelectronic devices often integrate/assemble dissimilar materials with different functionalities together on a nanometer scale, the control of the electrical integrity of the conglomerate becomes a formidable issue and is of paramount importance to the overall performance of the devices. Carrier transport in these structures is affected by the band alignment condition at many of the interfaces either directly in line of, or peripheral to, the conduction paths. The ability to control the band offset at solid interfaces, which is obviously a desirable and even necessary skill to master for these applications, however remains a capability we presently do not own. At metal-semiconductor (MS) interfaces, which constitute one of the most important classes of technological interface, the control of the band-offset, which is also known as the Schottky barrier height (SBH) at MS interfaces, has been difficult due to the well-known Fermi-level (FL) pinning phenomenon. Presently, the formation mechanism of the SBH still remains a subject of much debate [1, 2]. In the literature, there have been sporadic demonstrations that the magnitude of SBH can be moderately adjusted by altering the atomic structure of the MS interface, applicability of such a strategy is limited to very few (epitaxial) MS systems [3, 4]. Mechanisms by which empirical methods, such as varying the deposition temperature [5], the insertion of an interfacial insulator layer [6, 7], or the surface treatment by chacolgen [8], were able to change the SBH are not well understood, making these methods less reliable. In order to be able to systematically tune the SBH, its formation mechanism needs to be thoroughly understood [2, 9, 10].

1.1 Schottky Barrier Height

The Schottky barrier height, as one of the most interesting properties of the metal-semiconductor systems, governs the electronic transport across the MS interfaces, and therefore, is of vital importance to the successful operation of virtually all the semiconductor devices. When a metal and a semiconductor are brought into intimate contact, thermal equilibrium is established, as shown in Fig. 1. The SBH measures the energy difference between metal Fermi level and the majority band edge of the semiconductor. The first order theory of the barrier height was the original Schottky-Mott model [11, 12], based on the assumption of the charge distribution on the free surfaces of the isolated metal and semiconductor crystals being frozen during the formation of the MS interface. Within the non-interactive Schottky-Mott theory (SMT), the spatial gap between the metal and the semiconductor is envisioned to be reduced to zero, while the relative position of the bands of the semiconductor and the metal is assumed to remain unchanged. The resultant n-type SBH is given as:

$$\Phi^0_{B,n} = \phi_M - \chi_S, \quad (1)$$

where $\Phi^0_{B,n}$ is the SBH to an n-type semiconductor, ϕ_M is the work function (WF) of the metal, and χ_S is the electron affinity (EA) of the semiconductor. Because of its sound basis in the superposition principle of the electric potential, the SMT is valid whenever the rearrangement of charge during the formation of the MS interface can be ignored [9, 10]. The SMT predicts a strong dependence of the SBH on the metal work function:

$$S_\Phi \equiv \frac{\partial \Phi^0_{B,n}}{\partial \phi_M} = 1, \quad (2)$$

where S_Φ is known as the interface behavior parameter, or the S-parameter, of the semiconductor. Experimentally however, the SBH has been observed to be insensitive to the magnitude of the metal work function., and the S-parameter is usually found to be much smaller than unity [13]. A term, “Fermi-level (FL) pinning” [14], has been used to denote the insensitivity of the experimental SBH to the metal work function.

The failure of the non-interacting, Schottky-Mott model to account for experimentally observed SBH is well understood to arise from its neglect of metal-semiconductor interaction and the resultant, additional, interface dipole. Traditionally, the additional dipole has been modeled rigidly as the result of charge exchange between the metal and the surface/interface states residing on the semiconductor, over a fixed distance assumed to be the interface distance. In a simplified view adopted by many models, the surface/interface states are further assumed to be entirely a property of the semiconductor, leading to semi-quantitative explanation of

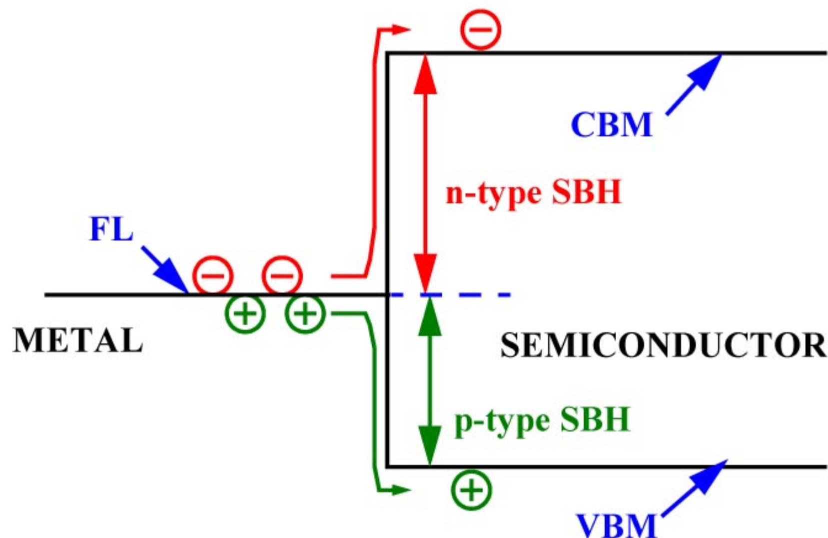

Figure 1. First order Schottky-Mott model of metal-semiconductor contacts.

experimentally observed FL pinning behavior [15-21]. However, the common assumption of the independence of the interface states on the metal, which underpins many "interface state models", does not agree with experimental results and has also been repeatedly dismissed by ab initio calculations. An alternative view on the formation of the interface dipole, cast without specific reference to interface states, focused on chemical bond formation at MS interfaces and showed that the expected bond polarization alone could account for the experimentally observed interface dipoles [9, 10, 22, 23]. Within the latter point of view, the interface dipole depends on, and therefore can be controlled by, the atomic structure of the interface. Also within the same vein, FL pinning can be attributed to interface equilibration, i.e. the formation of polarized interface bonds.

1.2 Interface Dipole

This lack of a strong metal dependence shows that the charge rearrangement at a typical MS interface is usually non-negligible and gives rise to an additional dipole $e\Delta_{MS}$ [9, 10], which modifies Eq. (1) to a more general form

$$\Phi^0_{B,n} = \phi_M - \chi_S + e\Delta_{MS} . \tag{3}$$

The existence of the non-negligible interface dipole causes the SBH to be weakly dependent or even independent on the metal work function, such that the SBHs for a semiconductor tend to converge in a narrow range [13]. The origin of the MS interface dipole is the focus of various theories, which as discussed above fall into two groups: one relying on the transfer of charge between metal and surface states of the semiconductor and the other focusing on the polarized bonds at the interfaces. It should be pointed out that the former mechanism is not sensitive to the

interface atomic structure and would predict little room for SBH tuning through structural manipulation, while the latter mechanism is very sensitively dependent on the interface bonds and could accommodate significant swings in the SBH with structural adjustments. Simply from the mounting experimental evidence for significant variations in the observed SBH under various fabrication conditions [3, 4] and the discoveries of large scale SBH inhomogeneity at most non-epitaxial MS interfaces, it seems clear that the formation of the interface dipole has strong

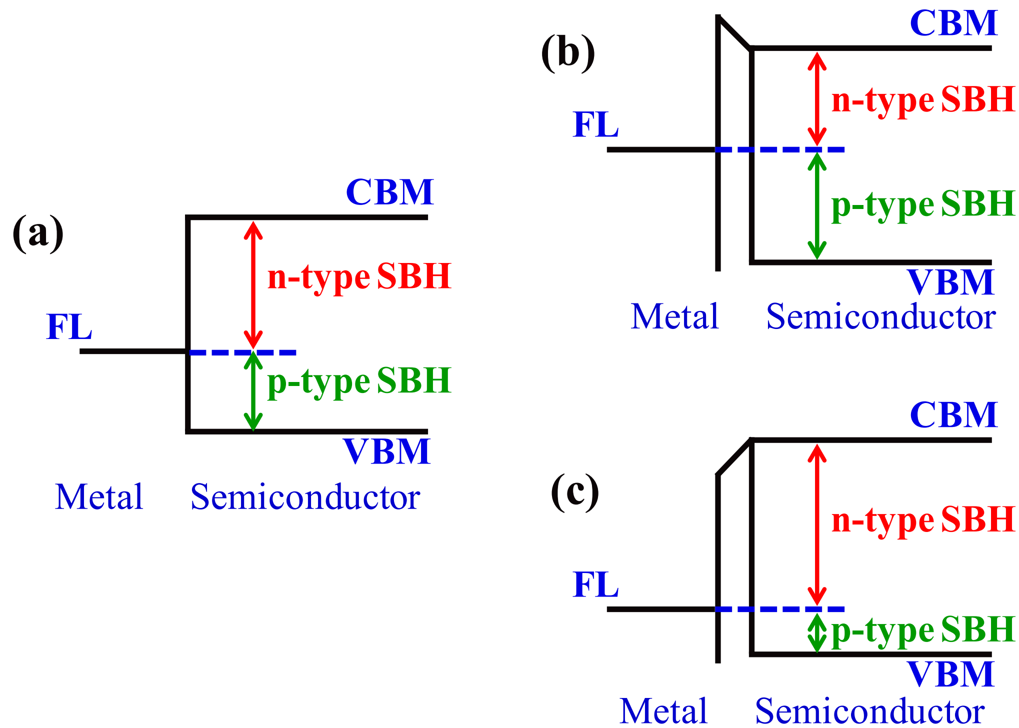

Figure 2. Schematic of interface dipole.

Comparing to (a) non-interactive direct contact, the presence of (b) a negative interface dipole, and (c) a positive interface dipole, results in (b) decreased n-type (increased p-type) SBH, and (c) increased n-type (decreased p-type) SBH. A negative dipole here is defined as one that is negative to the metal surface and positive to the semiconductor bulk.

structural dependency. Instead of being a property of only the semiconductor, the interface dipole has much to do with both parties and how they interact.

The polarity and the amount of charge transfer associated with a chemical bond usually follow the direction of electronegativity differential of the atoms in the bond. At a MS interface, the polarity of the interface dipole is thus expected to depend on the electronegativities of the metal and the semiconductor. As the ability to attract electrons, the electronegativity can be used to estimate the charge exchange across the MS interface. A simple model of interface electrical dipole can be illustrated as Fig. 2. In this document, the polarity of a dipole is defined as follows: a negative dipole is one which is negative away from the semiconductor and positive toward the semiconductor bulk. As shown in Fig. 2, the formation of a negative dipole at the MS interface will lower the energy band positions on the semiconductor side comparing to the metal side, which results in a decreased n-type (increased p-type) SBH with respected to the non-interactive model. Meanwhile, a positive dipole will have the opposite effect on the resulting SBH.

For a given pair of metal and semiconductor material, the interface dipole formation is largely a result of the minimization of interface energy. Within equilibrium thermodynamics, the ability to manipulate the interface structure and, in turns, the magnitude of the dipole is rather limited. An exception here is to artificially insert a layer of foreign materials, with the hope of leading to some metastable structure and a net overall dipole across the interface that is significantly modified from the original dipole.

1.3 Main Idea behind This Thesis

The presence of strong interaction at common MS interfaces, i.e. FL pinning is a major reason that SBH tuning is such a difficult task for covalent semiconductors. As bond polarization is likely the origin for dipole at the MS interfaces, the adjustment of SBH is difficult as the formation of chemical bonds is usually governed by thermodynamics. A possible strategy to circumvent the usual chemistry responsible for FL pinning, may be the artificial creation of designed interface structure under conditions far from equilibrium. The metastable structure thus created could then provide electrical properties unavailable from equilibrium structures. It is with the notion that the chemical stability of part of the interface structure may help the preservation of these partial structures at the full metastable interface that this project was launched.

A large body of research on SBH adjustment by insertion of dipolar organic molecules already exists in the literature [24-32]. While some remarkable results have been obtained in prior studies, the preparation of these molecules and surfaces required special techniques and environment that may be difficult to implement in semiconductor laboratories. In addition, organic molecules are known to suffer from low thermal stability, and coverage nonuniformity. Simply from the perspective of inducing a large dipole moment and possessing chemical and thermal stability, it seems that non-organic layers may be preferable. It is noted that several adsorbate-terminated semiconductor surfaces are highly stable chemically, and possess significant dipole moments. Surprisingly, the formation of Schottky barriers on these surfaces has never been systematically studied. The use of non-organic interlayer for SBH adjustment is the main idea behind this thesis work. In particular, several chemical stable ATS surfaces will be fabricated, and explored for SBH adjustment. The main theme of this project is the study of the effect of interfacial atomic layer on the SBH of this interface.

CHAPTER 2. Background

2.1 Partisan Interlayer

In a nutshell, an interfacial atomic layer (interlayer) at an MS interface is a single, atomically-sharp, layer of "foreign" atoms inserted between the semiconductor and the metal. From the perspective of modifying the overall interface dipole, the most relevant property of an

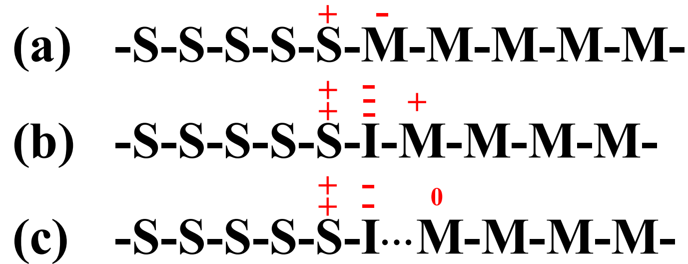

Figure 3. Schematic representations of atomic layers making up metal (M) – interlayer (I) – semiconductor (S) interfaces and the formation of interface dipole.

Interfaces formed as: (a) intimate MS interface; (b) interlayer bonded to both sides; (c) interlayer preferentially bonded to the semiconductor. Horizontal bars indicate bonding between atomic layer. The electronegativites are assumed to be in the order I > M > S. The numbers of signs are meant to roughly indicate the net charge associated with each atomic layer. Note that the interlayer in (b) attracts more electrons from S than M, giving rise to an overall dipole with the same sign as (a). Whether the magnitude of this dipole is larger or smaller than that in (a) depends on details of the chemical bonds. A similar ambiguity exists if the interlayer has a very low electronegativity or one that's intermediate between the metal and the semiconductor.

interlayer is the electronegativity of its atomic species. Without specific reference to the valence number, crystal structure, or the bond lengths in the interface region, how the overall interface dipole should vary with the electronegativity of the interlayer is not readily predictable from simple chemistry (see Fig. 3(b)). An implicit requirement for applying the concept of electronegativity to a system is thermal equilibrium, i.e. all atoms under discussion belong to the same molecule. As mentioned above, a possible strategy to escape equilibrium chemistry is to create metastable structures. When breakage in chemical bonds results in neutral "sub-systems" un-bonded to each other, the total dipole of the entire system becomes dominated by charge-transfers within "sub-systems". As an example, Fig. 3(c) depicts a "partisan interlayer" that is bonded only to the semiconductor, leaving the interlayer-metal (I-M) interface un-bonded or only weakly bonded. The lack of strong bonds between the interlayer and the metal (IM) translates to the absence of a large dipole across that interface, i.e. the "pinning" at that interface is weak. As a result, the overall dipole at the (S-I···M) interface is largely dominated by that of interlayer-semiconductor interface (IS) which may be large and adjustable through the choice of the interlayer. The "non-interacting" junction between an I-terminated semiconductor and a metal, depicted in Fig. 3(c), is exactly the type of interface the Schottky-Mott theory is well suited to describe. However, since the "partner" of the metal is the adsorbate-terminated semiconductor (ATS), it is the electron affinity of the latter, χ_{ATS}, that should enter into Eq. (2).

It is known that surface termination could affect the electronic affinity of a polar semiconductor, e.g. As- or Ga-terminated GaAs have different electron affinities on polar surfaces (larger for As-terminated surfaces than Ga-terminated surfaces). Additional adsorbates on top of polar or non-polar semiconductors are also expected to change the semiconductor electron affinity, as a result of the charge transfer between the adsorbate and the semiconductor.

Simply from general principles, one expects adsorbates that are more (less) electronegative than the semiconductor to increase (decrease) the electron affinity of the semiconductor. Since some ATSs are widely reported to be chemically stable, there is some expectation that interaction between these ATSs and the deposited metal could be absent or weak, under which condition, the Schottky-Mott relationship should approximately hold

$$\Phi_{B,n}^{ATS} = \phi_M - \chi_{ATS} + e\Delta_{M-ATS} \approx \phi_M - \chi_{ATS} . \tag{4}$$

In (4), $\Phi_{B,n}^{ATS}$ is the n-type SBH of an MS interface fabricated by deposition of metal on a pre-fabricated ATS surface, χ_{ATS} is the electron affinity of the ATS, which may be quite different from that for the bare semiconductor, and $e\Delta_{M-ATS}$ is the dipole due to charge rearrangement at the metal-ATS interface, which is expected to be small. The investigation of this hypothesis is the main focus of the present "partisan interlayer (PI)" method. Under idealized conditions assumed in the PI approach, Eq. (4) holds and the SBH can be tuned through: (a) a selection of the metal work function on a fixed ATS; (b) a choice in the ATS without changing the metal; and (c) a combination of both.

In addition to its technological goal of practically controlling the SBH, the PI method also serves a scientific purpose: to test the Schottky-Mott model under non-interactive condition. Experimental results from PI investigations could ultimately improve or modify our understanding on the SBH formation mechanism.

2.2 Adsorbate-Terminated Surfaces

The success of the partisan interlayer method depends on the avoidance of any significant metal-ATS interaction. Therefore, the practice of the PI should prefer an adsorbate that is at least capable of terminating the substrate into stable closed-shell surface electronic properties. The chemical stability of this surface structure is then relied upon to withstand interaction with metals. The adsorbate-terminated surface is the first step to the creation of a metastable interface structure with designable SBH.

To form a partisan interlayer, a precise amount of adsorbate is first deposited and processed to form an ATS surface, the structure of which is stable enough that it may withstand the subsequent deposition of metal. In terms of its ability to induce a large change in the overall interface dipole, the most critical property of the interface layer atomic species is its electronegativity, i.e. its ability to extract electron from (or donate electron to) either or both sides of the interface. Elements with larger electronegativities than that of the semiconductor, extracting electron from the semiconductor and forming a negative dipole (negative to the ATS surface and positive to the semiconductor bulk), result in an increased electron affinity for the ATS and consequently a decreased n-type, and an increased p-type SBH. On the other hand, elements with smaller electronegativities play the opposite way, by forming a positive dipole (positive surface, negative bulk), and an increased n-type (a decreased p-type) SBH is expected. The ability that a partisan interlayer of a selected element changes the charge distribution also depends on the total density of the atoms at the interlayer. In that respect, ATS surfaces that may be reproducibly formed and self-organized are preferred. The actual coverage of the adsorbate atoms on stable ATS surfaces may be self-regulated during preparation. From the literature, and consistent with the concept of “valence mending” [33], there are adsorbate-semiconductor

systems that are known to have chemically stable, closed-shell, electronic configurations. In this work, we choose as our main substrate the simplest and the most studied of all semiconductors, silicon, where a variety of adsorbate-covered surfaces have been well documented. In particular, the As-terminated Si(111)1×1-As [34-40], the S-terminated Si(100)1×1-S [33, 41], and the Cl-terminated Si(111)1×1-Cl [42-45], are outstanding candidates for the primary demonstration of the partisan interlayer method. The sketches of their structures are shown in Fig. 4. As (Group V), S (Group VI), and Cl (Group VII) also fill the columns that are to the right of Si on the periodic table. Because the Pauling's electronegativities of As (2.18), S (2.58) and Cl (3.16) are larger than that of Si (1.90), the expected transfer of electron from Si to the topmost As, S, or Cl

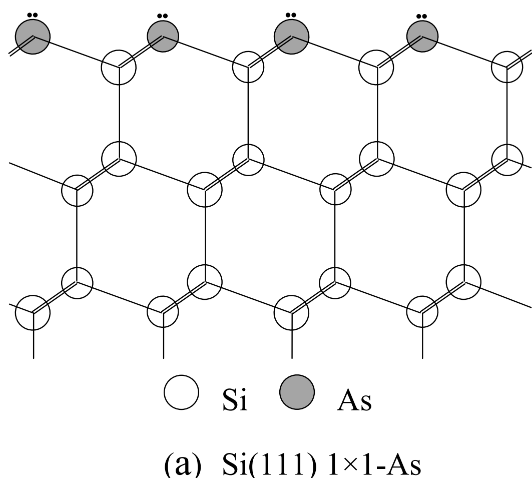

(a) Si(111) 1×1-As

Figure 4. Atomic structures of adorbate-teminated silicon surfaces.

(a) Si(111)1×1-As; (b) Si(100)1×1-S; and (c) Si(111)1×1-Cl.

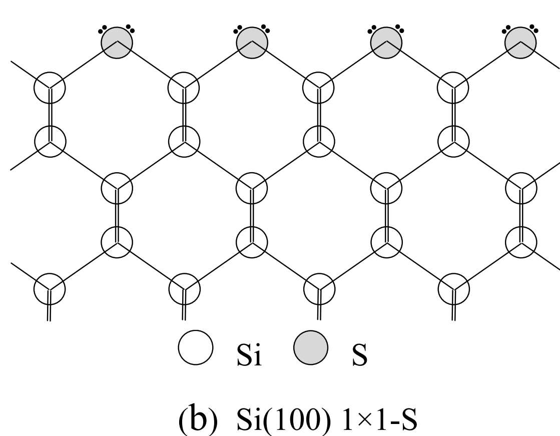

(b) Si(100) 1×1-S

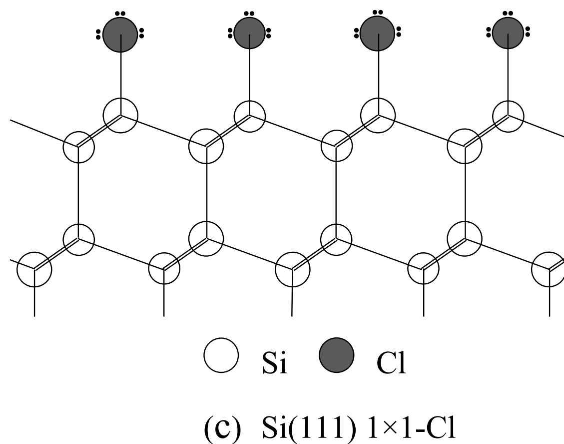

(c) Si(111) 1×1-Cl

layer should lead to an increase in the electron affinity of the adsorbate-covered substrates, compared to that of the clean Si(111) or Si(100) surfaces. Through the use of these ATS surfaces, demonstrated in this work, the SBHs on n-type Si are expected to be lower than that on clean Si, and p-type SBHs are expected to be higher than clean Si.

As shown in Eq. (4), a quantity of great interest from the perspective of SBH formation is the electron affinity of the semiconductor. For the ATS surfaces selected in our study, the electron affinity is largely unknown. Although the increased electron affinity of these ATS surfaces can be easily predicted from above reasoning, the magnitude of the change has not been estimated. In parallel to the experiments I am about to describe, theoretical electronic structure calculations were carried out in our laboratory. As the theoretical results are relevant for the present work, some description of these unpublished theoretical results is here briefly summarized.

These calculations used the adsorbate-covered Si surfaces in a symmetric slab configuration, within a three-dimensional periodic supercell [46]. All calculations were performed with at least 7 atomic layers of silicon for the (100) slabs and at least 8 atomic layers (4 bi-layers) of silicon for the (111) slabs. Adsorbates are introduced to both faces of the slab and vacuum with a minimum width equivalent to 15 atomic layers is used to separate the periodic slabs in the supercell geometry. The two outermost atomic layers on each surface are allowed to undergo relaxation in their vertical coordinate (z), through energy minimization. The Kohn-Sham equations of the density function theory (DFT) were solved using the plane-wave approach as implemented in the Vienna ab initio simulation package (VASP) [47, 48]. The local density approximation (LDA) was employed for the exchange-correlation functionals. Different surface terminations lead to very different distribution of charge near the surfaces, resulting in slight

Table I. Ab initio DFT calculations in the slab geometry.

	Slab Surface Termination	Average Interior Potential Energy (eV)	Electron Affinity Shift (eV)
Si(111)	Si(111)1×1-H	-10.60	-0.21
	Si(111)7×7	-10.81	--
	Si(111)1×1-As	-11.21	+0.40
	Si(111)1×1-Cl	-11.63	+0.82
Si(100)	Si(100)2×1	-11.23	--
	Si(100)1×1-S	-11.68	+0.45

shifts in the electrostatic potential inside the slab. Compared with the bare Si slab, the electrostatic potential energies for the adsorbate-covered surfaces are rigidly shifted, although the oscillatory nature of the Si bulk crystal has remained largely unchanged. These rigid shifts are the item of main interest in these calculations, as they represent the net effect of charge transfer during surface dipole formation, summarized in Table I.

The measurement of the change in electron affinity is not readily achievable under our experimental capabilities. However, systematic trend in electron affinity can be approximately revealed through a study of the work function variation with the respective surfaces. Ideally, if the surface Fermi-level is not pinned, the work function of a heavily-doped n-type substrate should be close to the electron affinity of the surface, and the work function of a heavily-doped p-type substrate should be close to the ionization potential of the surface. However, as experiments showed, the Fermi-level of clean Si is usually pinned, e.g. at ~0.63 eV above the valence band maximum for Si(111)7×7 [49]. In the absence of exact knowledge of the FL position of the ATS surfaces, experimental determination of the electron affinity has to rely on indirect deductions. To get a better appreciation for the change of the surface electronic properties into adsorbate, work function experiments were conducted for both n- and p-type

substrates. The change in the electron affinity is then experimentally estimated as the average change of n- and p-type work function. The non-destructive Kelvin Probe (KP) technique measures the contact potential difference (CPD) between the probe tip (with known material and work function) and the sample surface, which is the ideal tool for the present study.

2.3 Metal

From the perspective of involving a wide range of metal work functions, In (4.12 eV), Ag (4.26 eV), and Au (5.1 eV) [50] are chosen to form the SBH on the ATS's mentioned above. The absence of silicide phases in their binary phase diagrams with Si and the ease with which these metals can be evaporated in vacuum make these three metals ideal candidates for our investigation.

Additionally, Ag has been well recognized as one of the very few metals that form non-interactive junctions with Si, likely because of the closeness of its electronegativity (1.93) to that of Si (1.90). Such similarity implies that the $e\Delta_{MS}$ term in Eq. (3) should be small for the intimate Ag-Si junction. Only under such a condition can the change in the SBH induced by the interlayer, i.e. the difference between Eqs. (1) and (4), be directly compared with the change in the electron affinity of the semiconductor.

CHAPTER 3. Experiment

Both n- and p-type, (111)- and (100)-oriented Si substrates, with doping concentration ~10^{15} cm^{-3}, were used in this study. The (111) substrates were pre-fabricated by heavily doping the back side, while the (100) substrates were 5~10 µm lightly-doped suface epitaxial layers on heavily-doped wafers, such that the ohmic contacts could be made directly on these heavily doped back sides and were found to be of equally high quality as those made by additional metal evaporation. The wafers are cut into rectangular shapes of 1.5×2.5 cm^2 in dimension for the purpose of sample transferring and mounting.

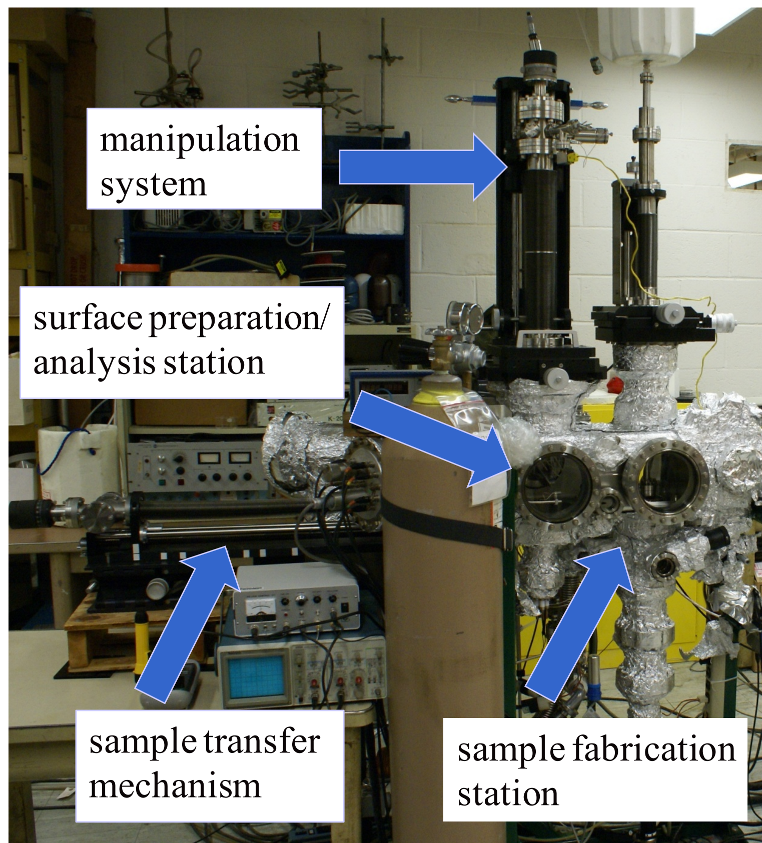

Figure 5. A picture of the dual-station ultra-high vacuum chamber constructed for the present experimental work.

3.1 UHV Chamber

The best possible condition under which this experimental work can be carried out is a clean environment with seamless transfer mechanism. A dual-station ultra-high vacuum (UHV) system, shown in Fig. 5, with base pressure in the 10^{-10} torr range, was designed such that the preparation of adsorbate-terminated silicon surfaces and the in-situ fabrication of Schottky diodes were performed without breaking the vacuum. In addition, this chamber was equipped with Auger Electron Spectroscopy (AES), Low-Energy Electron Diffraction (LEED), and Kelvin Probe (KP) for surface analysis. An ion pump was employed as the primary pumping power to provide the silence environment, which is crucial to the successful KP measurement. A Residual Gas Analyzer (RGA) was also installed to indirectly monitor the evaporation rate of the

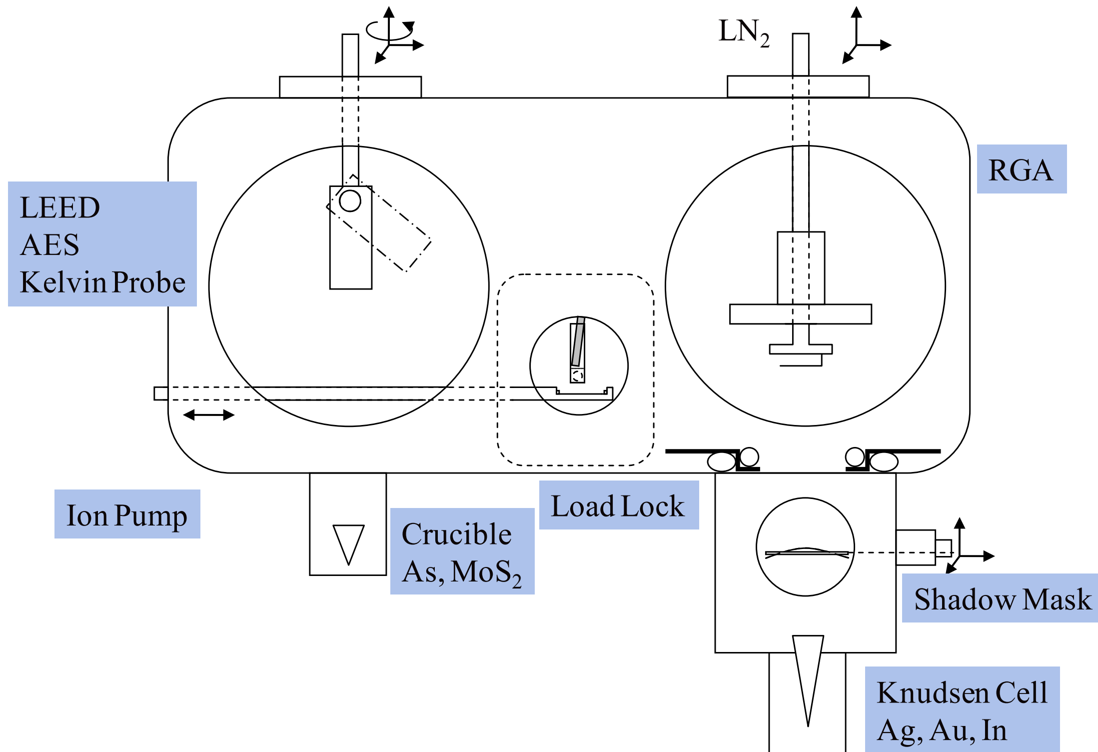

Figure 6. Structural view of main components installed in the UHV system.

adsorbate source while the surface modification went on. As for the metallization source, a Knudsen Cell provided best control over temperature in order to obtain calibrated evaporation rate and constant deposition thickness. The main components and the structure of the chamber are sketched in Fig. 6.

In addition to these vacuum equipments and surface characterization tools that can be purchased and are commonly found on many UHV systems, the UHV chamber employed for the present work has many home-designed and locally machined features and functions especially tailored to our experimental needs. Some of the modifications/additions that I have been personally responsible for or deeply involved with are individually discussed below.

3.1.1 Shadow Mask Mounting

To make Schottky diodes with precise areas, a shadow mask is usually employed. Traditionally, the sample has to be mounted to a sample holder under the shadow mask before being transferred into the vacuum chamber, which could not be adopted in the present experiments since the surface modification had to take place before fabrication of the diodes. If the mask remains in the chamber, the sample has to be aligned extremely well to make the

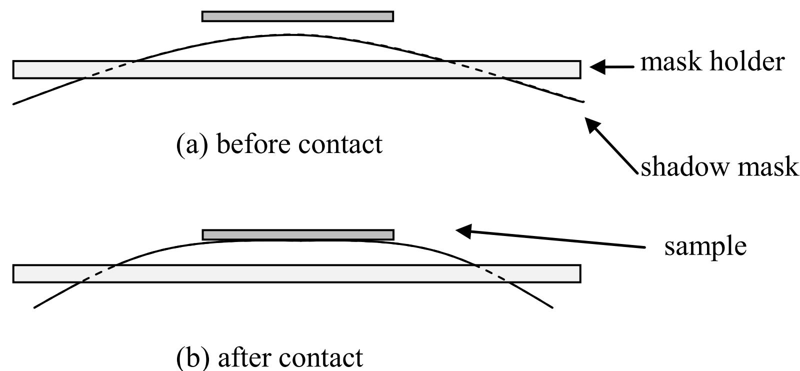

Figure 7. Shadow mask mounting mechanism.

intimate contact everywhere, or the diodes would have fuzzy edges that cause leakage currents. From this concern came the following mask contact idea.

In this work, the shadow mask was crafted with copper-stainless steel to a thickness of ~5 mil, which provided the spring-like flexibility with which to mount the mask on a holder in the way shown in Fig. 7(a). When the sample comes in contact, as shown in Fig. 7(b), the mask presses the sample tight enough so that a sharp edge of the diode is guaranteed. The flexibility of the mask material also allows it to rebound for reuse.

In addition, the mask holder was installed on an XYZ manipulator which allowed adjustment of position to meet the sample, and even removal of the entire mask for making large area back ohmic contact.

3.1.2 Isolated Fabrication Vessel

In the UHV chamber for the present work, the sample was transferred from the surface

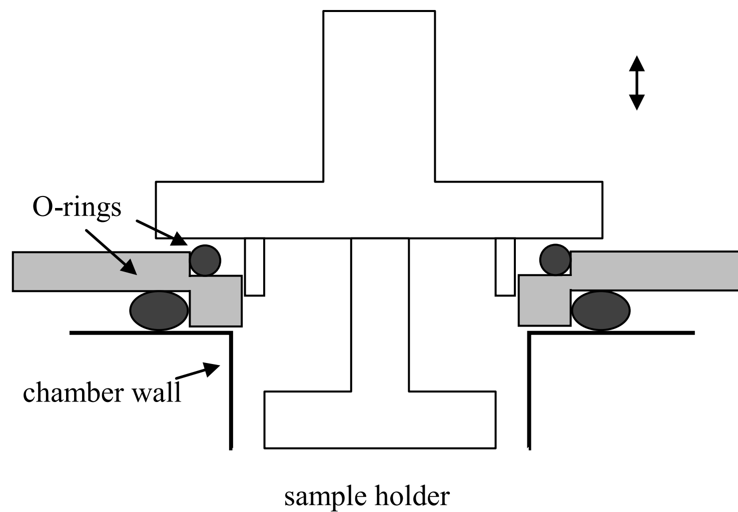

Figure 8. Isolation settings for the fabrication station.

modification station to the fabrication station without breaking the vacuum. However, the metallization process inevitably evaporates contaminants which could contaminate the surface analysis components (LEED, AES). Therefore, it was necessary to isolate the fabrication vessel during the process. Fig. 8 shows how this was done without complicated valves. The metal deposition took place in a lower chamber and an additional housing outside the sample holder provided the sealing ability with the help of two Viton O-rings. The entire sample holder was installed on an XYZ manipulator for adjustments, where the vertical motion pressed the O-rings to make the seal.

3.1.3 Sample Transfer Mechanism

Another critical part was the connection, between the UHV chamber and outside, and between the modification and fabrication stations. A steady transfer of sample was so important to the efficiency. Dropping a sample on the way was simply depressing because a lot of time and

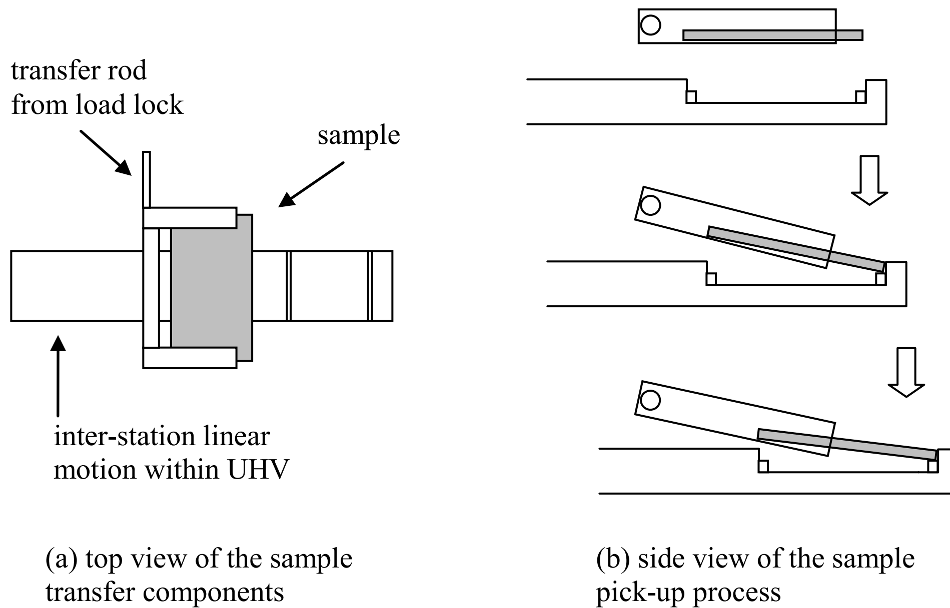

Figure 9. Sample transfer and pick-up mechanism.

work had been invested before the run, not even mentioning that a sample could fall into some components and cause malfunction of the system. A magnetic transfer rod was tested unreliable for this job due to its shaky nature. As shown in Fig. 9, a sample-holding platform was installed on a long-travel inter-station linear shift with UHV-grade bellows. The sample came in from the load lock in an envelope-like holder on a magnetic transfer rod. The stability of the transfer rod was not an issue since the sample was positioned vertically before being flipped horizontally for pick-up, as Fig. 9(a) shows. The actual pick-up process took place in a way shown in Fig. 9(b). This was a simple design which had not only the stability, but also the ability to deliver the sample precisely to anywhere along the axis. An additional feature of this mechanism was that the sample could be flipped upside-down, for the purpose of back side metal deposition when needed, by simply practicing the procedure in Fig. 9(b) reversely to move the sample back into the "envelope" and picking it up on the other side.

3.1.4 Glass Reactor

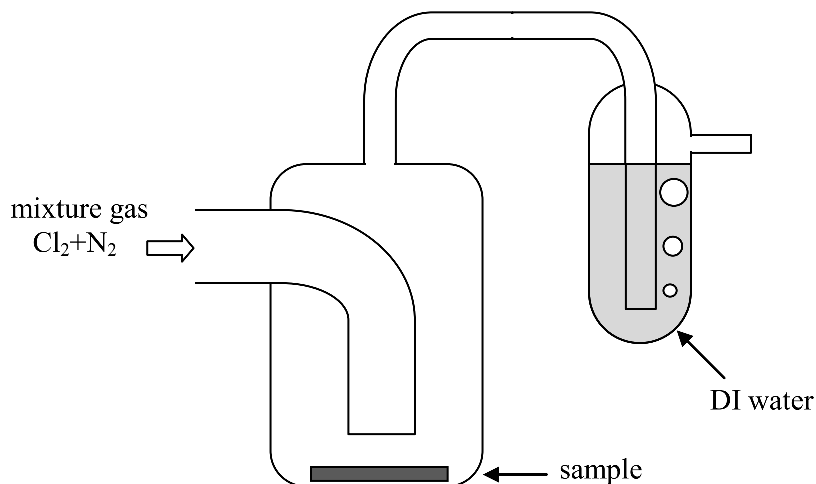

Figure 10. Glass reaction system for the gaseous-phase Cl-termination process.

The Cl-termination process was done ex situ in a glass reactor, shown in Fig. 10, for the purpose of protecting the stainless steel chamber from corrosive chlorine gas. The mixture gas was delivered directly to the Si surface while the water bubble monitored the gas flow which was kept at approximately a certain rate. The main body of the reactor was merged in an oil bath for heating purpose.

3.2 Experimental Procedures

All samples received standard RCA cleans to form protective Shiraki oxide[51] on Si substrates, before further surface treatments. The detailed cleaning process is as follows:

(1) wash in Acetone with agitation (ultrasonic) to remove photoresist, if any;

(2) brush with Triton;

(3) rinse in overflowing de-ionized (DI) water for 10 minutes;

(4) rinse in Methanol for 5 minutes with agitation;

(5) boil in Trichloroethylene (TCE) for degreasing;

(6) repeat (4) then (3);

(7) dip in HF to remove native oxide, then rinse in DI water;

(8) boil in a solution of NH_4OH:H_2O_2:H_2O (1:1:3) at 90 ºC (bring mixture of NH_4OH and H_2O to the temperature first and add H_2O_2 just prior to use) for 10 minutes to form thin surface oxide, followed by (3);

(9) dip in diluted HF (2.5%) for 15 seconds to remove the oxide, followed by (3);

(10) boil in a solution of HCl:H_2O_2:H_2O (1:1:3) at 90 ºC (bring mixture of HCl and H_2O to the temperature first and add H_2O_2 just prior to use) for 10 minutes to form thin surface oxide, followed by (3) and (9);

(11) boil in a solution of HCl:H_2O_2:H_2O (3:1:1) at 90 ºC (bring mixture of HCl and H_2O to the temperature first and add H_2O_2 just prior to use) for 10 minutes to form Shiraki oxide;

(12) rinse and keep in DI water for future use; blow dry with Nitrogen before use.

After the above cleansing, the samples were used to prepare the following surfaces:

(a) Clean Si(111)7×7 structure was obtained by heating at 900 ºC for 10~30 seconds in UHV to remove the protective oxide [51];

(b) The Si(111)1×1-As structure was formed by holding the clean 7×7 surface from 600 ºC down to 350 ºC in a stream of arsenic for 5 minutes [34];

(c) The Si(111)1×1-H surface was obtained by removing the oxide ex-situ with buffered HF (NH_4F:HF~7:1, pH~5) for 15 seconds [52];

(d) The Si(111) 1×1-Cl structure was obtained by exposing H-terminated surface to Cl_2/N_2 mixture gas (0.4% Cl_2 + 99.6% N_2) at 150 ºC in the glass reactor shown in Fig. 10, for 15 minutes [42];

(e) Clean Si(100)2×1 structure was obtained by flashing off the protective oxide in UHV, similar to (a);

(f) The Si(100)1×1-S surface was formed by holding the clean Si(100)2×1 surface at room temperature for 20 min in a stream of sulfur molecules [41], generated from a thermally-heated MoS_2 source, followed by heating up to 350 ºC for 2 min to remove excessive sulfur.

After chemical preparation ex situ, Cl- and H-terminated substrates were quickly loaded into UHV chamber and were degassed at 350 ºC for 5 minutes before surface analysis.

On a typical run, a sample was first placed in the load lock, specifically, in the envelope-like sample holder (in Fig. 9) on the magnetic transfer rod. After reaching lower 10^{-6} torr, the

load lock was open to the UHV and the sample was picked up by the steady transfer rod (also in Fig. 9) and mounted to the surface preparation/modification station. Before surface analysis Cl- and H-terminated substrates were degassed at 350 ºC for 5 minutes, while S- and As-terminated surfaces were obtained right in the modification station. After the desired surface structure was confirmed by LEED and AES, the sample was then released from the modification station back to the steady transfer rod and delivered to the sample holder at the fabrication station. The sample was hung loose, facing downward, when the sample holder was moving down to the lower metallization chamber until the seal was made (see Fig. 8) to isolate the lower chamber. The shadow mask then pressed the sample tightly (see Fig. 7) against the ceiling of the sample holder. It was optional to have the sample holder at room temperature or keep it cooled with liquid Nitrogen for low-temperature-substrate deposition. Circular diodes of In, Ag or Au, with diameters of 0.05 mm to 2.0 mm and film thickness of approximately 250 nm, were fabricated on Si with different surface structures, by thermal evaporation from the Knudsen cell and through the shadow mask. The sample was then released from the shadow mask and removed from the lower chamber. If a back ohmic contact was needed, the sample could be flipped through the cooperation of both transfer rods again and sent back to the lower chamber for the metal deposition, with shadow mask removed completely out of the way; otherwise, the sample would be retrieved through transfer rods and load lock, and ready to test.

Electrical characteristics of diodes were studied in a cryogenic four-probe station (base pressure $<10^{-6}$ torr) which was capable of maintaining the sample at from 77K to 400K, and by Agilent B1500A Semiconductor Device Analyzer which was capable of running programmable current-voltage (I-V) and capacitance-voltage (C-V) characteristic continuously without having to switch cables.

3.3 Surface Characterization

All six types of surfaces prepared above were of excellent quality, indicated from the robust and clear LEED patterns in Fig. 11, with respect to the same numbering above. AES analysis revealed detectable but negligible amount of common carbon and oxygen contaminants on these surfaces except those clean ones. AES analysis also showed that the amounts of S- and Cl-coverage were typically 1.0 monolayer, consistent with their predicted surface structures. As-coverage was instead determined by Rutherford Backscattering Spectrometry (RBS) with a 2

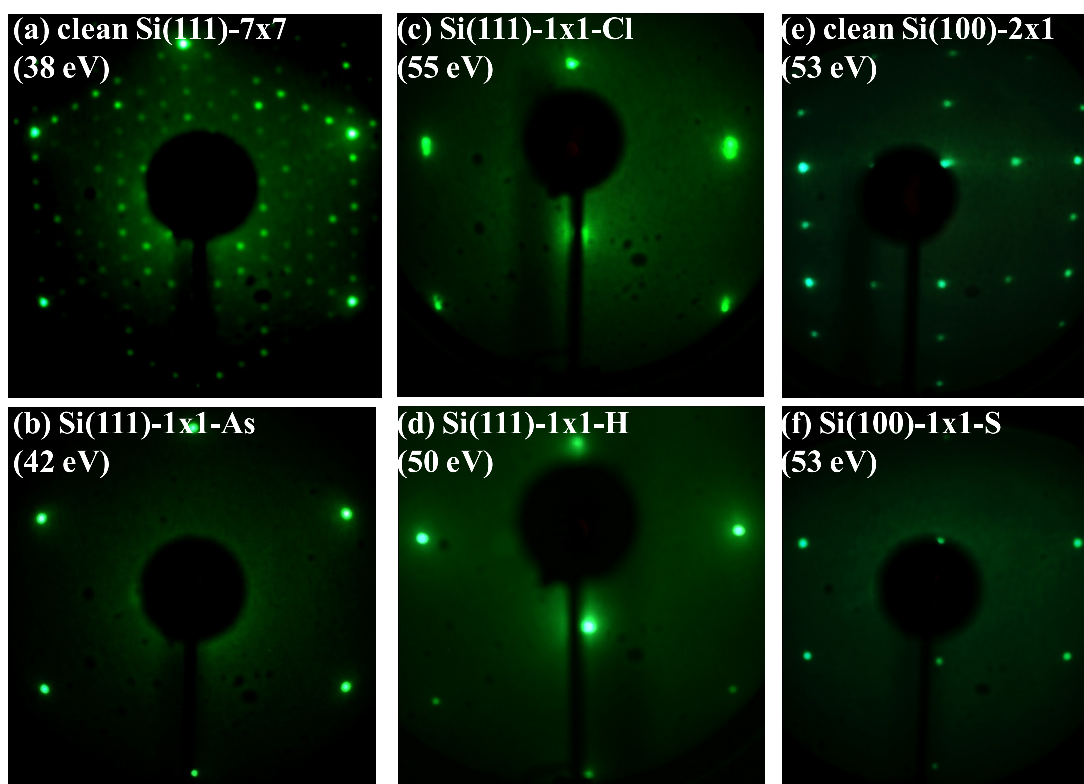

Figure 11. Representative LEED patterns.

(a) clean Si(111)-7×7 at 38 eV, (b) Si(111)-1×1-As at 42 eV, (c) Si(111)-1×1-H at 50 eV, (d) Si(111)-1×1-Cl at 55 eV, (e) clean Si(100)-2×1 at 53 eV, and (f) Si(100)-1×1-S at 53 eV.

MeV He beam after a thin layer of metal was deposited on top, and was also found to be 1.0 monolayer as expected.

3.4 Electrical Measurement

An extensive study of the temperature-dependent electrical characteristics of SB junctions fabricated on various starting surface structures was carried out. Capacitance-voltage measurements were conducted only at low temperatures, for the purpose of low series resistances, and under reverse bias to reduce the influence of in-phase currents. Since the depletion-layer capacitance per unit area, C_D, has the following relationship with the applied voltage, V_a:

$$\frac{1}{C_D^2} = \frac{2\left[V_{bi} - V_a - \left(k_B T / e\right)\right]}{e\varepsilon_S N_D}, \tag{5}$$

where V_{bi} is the "built-in" voltage, and N_D is the doping concentration. The built-in voltage can be determined by the linear extrapolation of $1/C^2 - V_a$ plot to the voltage axis, and an n-type SBH is then:

$$\Phi_{B,n}^0 = eV_{bi} + eV_n + k_B T, \tag{6}$$

where V_n is the difference between the Fermi level and the conduction band minimum for a neutral semiconductor. Moreover, the doping concentration can be determined by the slope of the same plot:

$$N_D = \frac{2}{e\varepsilon_S}\left[-\frac{1}{\partial\left(1/C^2\right)/\partial V_a}\right]. \tag{7}$$

The current-voltage relationship of a SB junction is described by the thermionic emission theory as

$$J\left(V_a\right) = J_S\left[\exp\left(\frac{eV_a}{nk_BT}\right) - 1\right], \tag{8}$$

where J is the current density under such applied bias, J_S is the saturation current density, and n is the ideality factor. By fitting the experimental I-V trace into Eq. (8), one can find the ideality factor, and the value of the saturation current, from which the SBH values can be calculated:

$$J_S = A^{**}T^2 \exp\left(\frac{-\Phi_B}{k_BT}\right) \tag{9}$$

where A^{**} is the Richardson constant, and Φ_B is the SBH at this certain temperature. The junction currents can be further studied with Activation Energy (AE) analysis, where the SBH's were deduced from the negative slope of the "Richardson plot" of the logarithm of I/T^2 against $1/k_BT$, according to Eq. (8).

CHAPTER 4. Electron Affinity of Adsorbate-Terminated Silicon Surfaces

Heavily doped n- and p-type Si substrates were prepared by the same procedures above without metal deposition, for work function measurement, carried out in situ with KP. To minimize systematic errors and difficulties associated with absolute work function measurement in UHV [53, 54], measurements were always conducted in tandem for two different surface structures fabricated on the same substrate, with the emphasis placed on the difference between the two measurements. Specifically, the work function of an adsorbate–terminated surface was first measured, followed by the measurement of the clean Si obtained on the same substrate after flashing off the adsorbate. From the Kelvin Probe measurement, the work function of the clean Si surface was consistently measured to be independent of substrate doping. This is in agreement with the literature that the FL is firmly pinned for the Si(111)7×7 surface [49], at ~0.63 eV above the valence band maximum. To minimize systematic errors, WF for each ATS surface was measured in conjunction with that of a clean surface fabricated on the same substrate. The differences between these back-to-back measurements are listed as $\phi_{ATS} - \phi_{\text{clean}}$ in Table II, in comparison with the theoretical results. To actually deduce the EA of a particular ATS surface from WF data, one needs information on its surface FL position, which for these ATS surfaces is largely unknown. The determination of the electron affinity is further hindered by an absence of strong FL pinning, at least for the Si(111)-Cl surface, as revealed by the variation of the WF with the substrate doping, as shown in Fig. 12. One notes that such a "weakening" of the FL pinning is expected for the present ATS surfaces, due to the removal/reduction of surface dangling bonds by the adsorbates. Despite these difficulties, the fact that the surface FL cannot fall outside the band gap firmly sets a lower limit, $\chi_{1\times1-Cl} - \chi_{7\times7} > 0.42$ eV, for the Si(111)-Cl. If one further makes the assumption that the charge neutrality level (CNL) of surface states for the ATS

Table II. Work function/electron affinity of adsorbate-terminated Si.

WF or EA (eV)	Si(111)1×1-As	Si(100)1×1-S	Si(111)1×1-Cl	Si(111)1×1-H
$\phi_{ATS} - \phi_{clean}$ expt. (n)	0.27	0.14	0.61	-0.28
$\phi_{ATS} - \phi_{clean}$ expt. (p)	0.33	0.12	1.05	0.12
$\chi_{ATS} - \chi_{clean}$ expt.	(0.30)	(0.13)	(0.83)	(-0.07)
$\chi_{ATS} - \chi_{clean}$ theory	0.40	0.45	0.82	-0.21

surfaces is unchanged from that of the clean Si, the increases of WF, for each ATS, on n- and p-type substrates (Table II) may be averaged to give an estimate of the increase in EA. Included in Table II, in parentheses, are these estimates, which, although lacking in scientific rigor, are not

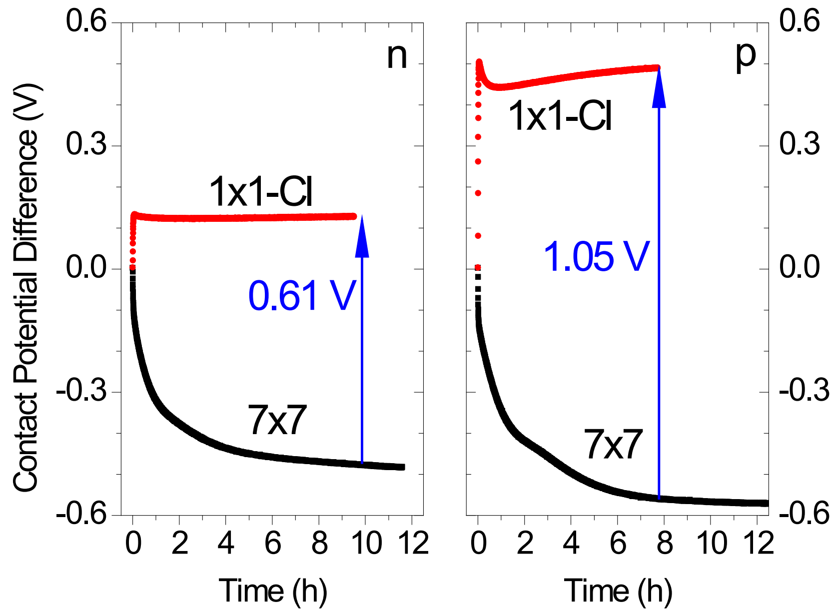

Figure 12. Kelvin Probe measurement of work function change by Cl-termination on Si(111).

Contact potential difference (CPD) is with respect to the reference electrode: $\phi = \phi_{ref} + CPD$.

unreasonable for the following reason. The dominant defects on the ATS surfaces are likely Si dangling bonds, as on the clean 7×7. It thus appears plausible that the CNL of the ATS surfaces may be placed similarly to that for the clean 7×7. Similar analyses were performed on Si(111)-As, Si(100)-S, and Si(111)-H surfaces, based on Kelvin Probe measurements shown in Fig. 13.

Contamination could have contributed to differences in the different reports. It should be mentioned that an increase in work function is suggestive of, although not equivalent to, a similar increase in electron affinity, due to possible shift in the FL position in the gap.

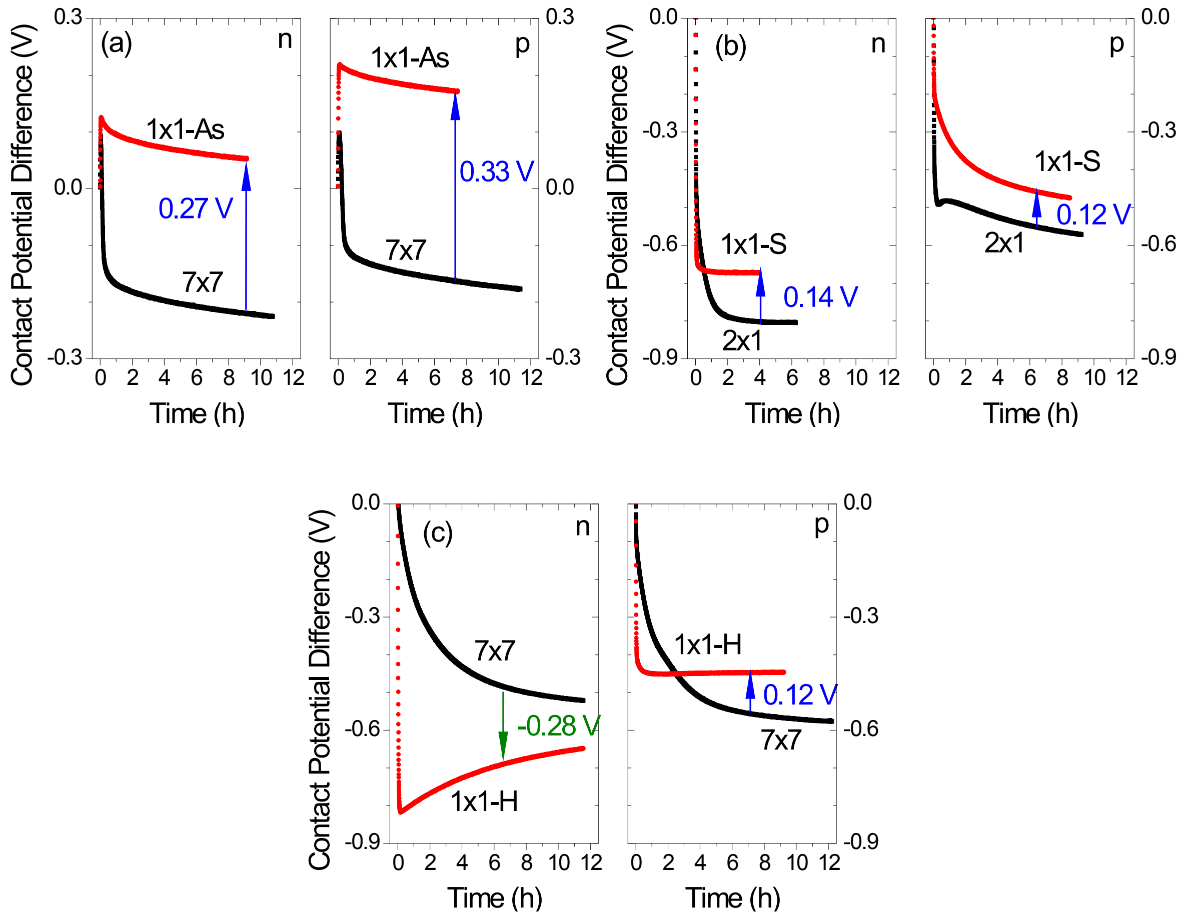

Figure 13. Kelvin Probe measurements of work function change by (a) As-termination on Si(111), (b) S-termination on Si(100), and (c) H-termination on Si(111).

CHAPTER 5. Controlled Modification of Schottky Barrier Height by Partisan Interlayer between Ag and Si(111)

To demonstrate the significant effect and the systematic trend of tuning the SBH on the same substrate and even without changing the metal, through the partisan interlayer approach [55], Si(111) was selected since multiple ATS structures were available on this particular substrate, such as As-, Cl- and H-terminated Si(111). Ag was chosen as the Schottky barrier metal because of an absence of thermodynamic driving force to react with the two ATS surfaces. Specifically, no binary compounds exist in the Ag-As phase diagram [56] and the Ag-Cl heat of formation (127 kJ/mol) is much smaller than the Si-Cl bond energy (406 kJ/mol) [57]. Additionally, the similarity between the electronegativities of Ag (1.93) and Si (1.90) implies that the $e\Delta_{MS}$ term in Eq. (3) should be small for the intimate Ag-Si junction. Only under such a condition can the change in the SBH induced by the interlayer, i.e. the difference between Eqs. (3) and (4), be directly compared with the change in the electron affinity of the semiconductor. The hydrogen terminated Si(111) 1×1-H surface is also studied in the present work, for comparison. However, it is unlikely that much of the H-Si structure can survive a metal deposition. Specifically, the surface structures of the subject in this chapter are the clean Si(111)7×7, the Si(111)1×1-As, the Si(111)1×1-Cl, and the Si(111)1×1-H.

In comparison to clean Si(111)7×7 surface, the shift in electron affinity on the ATS surfaces were deduced from the change in work function measured on both n- and p-type substrates, as demonstrated in Chapter 4. While the excellent numerical agreement between the experimental measurement and theoretical calculation, on the adjustments of the electron affinity by terminating the Si(111) surface with As, Cl and H, in Table II may be viewed as fortuitous,

overall it seems clear that the electron affinities of the Si(111)-As and the Si(111)-Cl surfaces are considerably higher than that of the clean Si(111).

An extensive study of the temperature-dependent I-V characteristics of Schottky barrier junctions fabricated on various starting surface structures was conducted. Representative I-V curves, obtained at a single temperature are shown in Fig. 14. Strikingly, the current densities for Schottky barriers fabricated on ATS substrates differ from that for clean Si surface by many orders of magnitude. The SBH values as calculated from the thermionic emission theory [2] are summarized in Table III. While the SBH on nominally H-terminated Si(111) remained close to that on the clean 7×7, decreases in the n-type SBH of as much as ~0.40 eV for As-terminated Si and ~0.22 eV for Cl-terminated Si were observed, compared with the 7×7. Correspondingly, the p-type SBH increased by ~0.27 eV for Si(111)-As and ~0.37 eV for Si(111)-Cl.

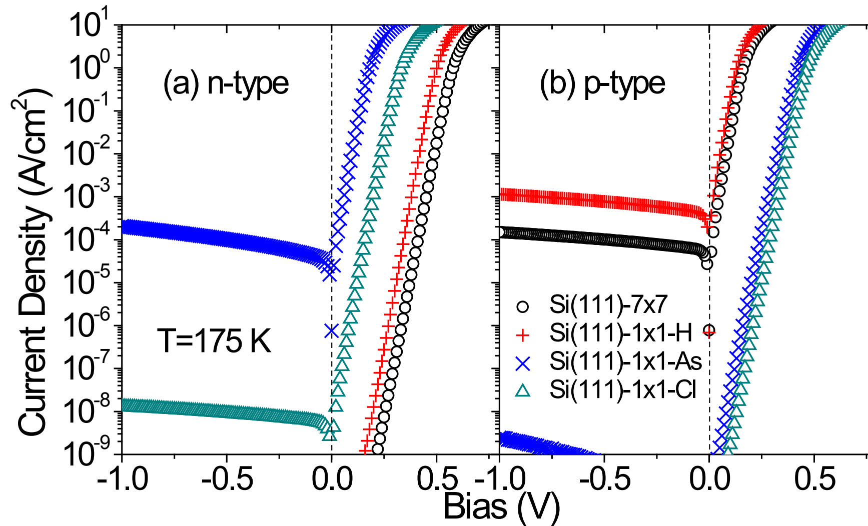

Figure 14. Experimental I-V curves, obtained at 175 K, for Schottky diodes fabricated on clean, H-, As- and Cl-terminated Si (111) surfaces: (a) n-type (b) p-type.

It should be noted that even though I-V traces behaved linearly on the semi-logarithmic plot for many decades, the ideality factors were found to consistently exceed unity (typically 1.05-1.15 at 300K), indicative of some degree of non-uniformity in the SBH [58]. Selected I-V curves at various temperatures from all types of ATS surfaces formed on Si(111) substrate are shown in Fig. 15. The ideality factors, obtained by fitting each individual curve into Eq. (8), are included at all temperatures. Specifically, the n-Si(111)7×7-Ag and p-Si(111)1×1-As-Ag

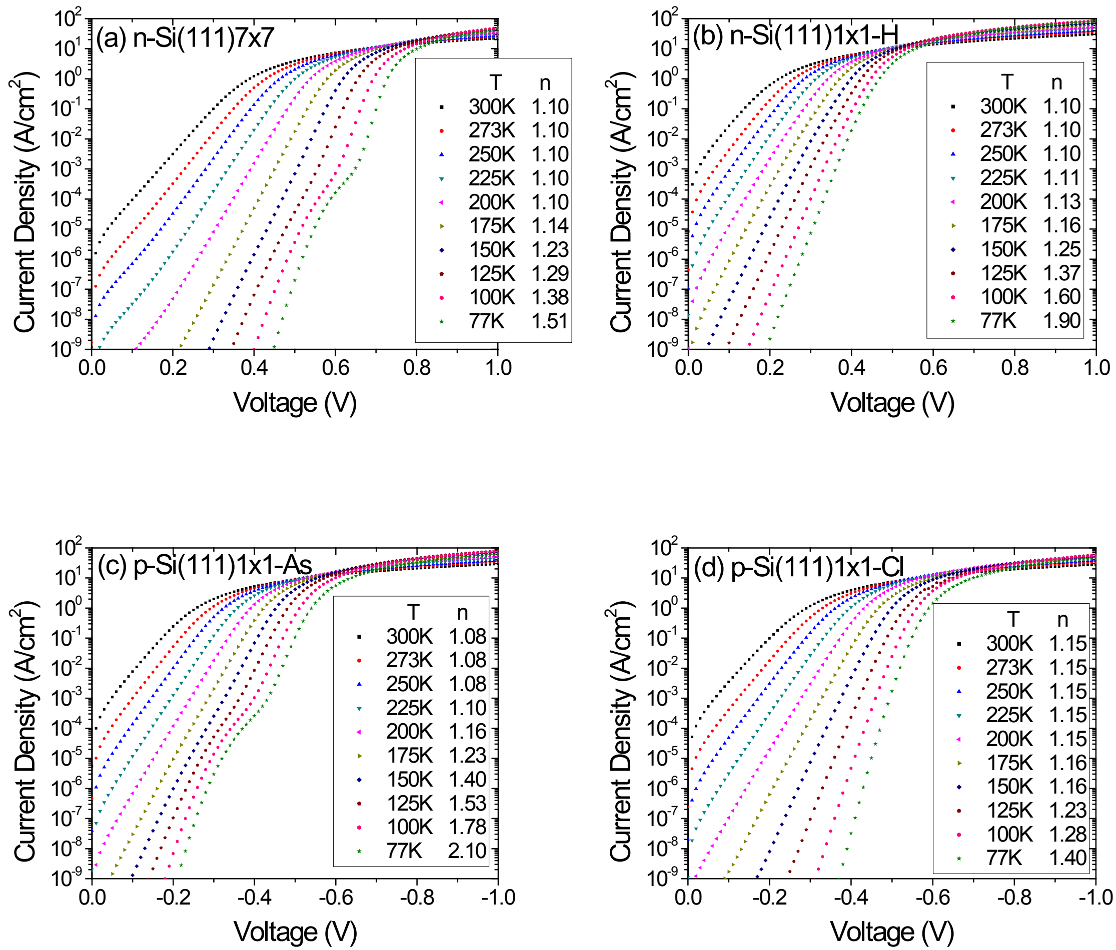

Figure 15. Representative I-V curves under forward bias from Schottky diodes of Ag on (a) clean, (b) H-terminated, (c) As-terminated and (d) Cl-terminated Si(111) surfaces, showing ideality factors at each individual temperature.

Schottky junctions, shown in Figs. 15(a) and 15(c), respectively, are indicative of sharply distributed low-SBH patches at the interfaces, while n-Si(111)1×1-Ag and p-Si(111)1×1-Cl-Ag diodes, shown in Figs. 15(b) and 15(d) respectively, are displaying a broad distribution of SBH variation at those interfaces, according to the successful model of electron transport at MS interface [58].

The activation energy (AE) method was used to analyze the saturation currents of the Schottky barriers on different surfaces. Richardson plots for all types of interfaces studied in this chapter are shown in Fig. 16, where the negative slopes of the plots at high temperatures provide direct comparison of the nominal SBH at these interfaces and on each doping type of the substrate. A straight fit at high temperatures is usually observed, except for some low-SBH junctions where series resistances start to dominate the total currents when temperature raises. However, almost every plot tends to flatten and display a tangent with a considerably lower SBH at lower temperatures than that characteristic of the rest of the curves. These lower values could

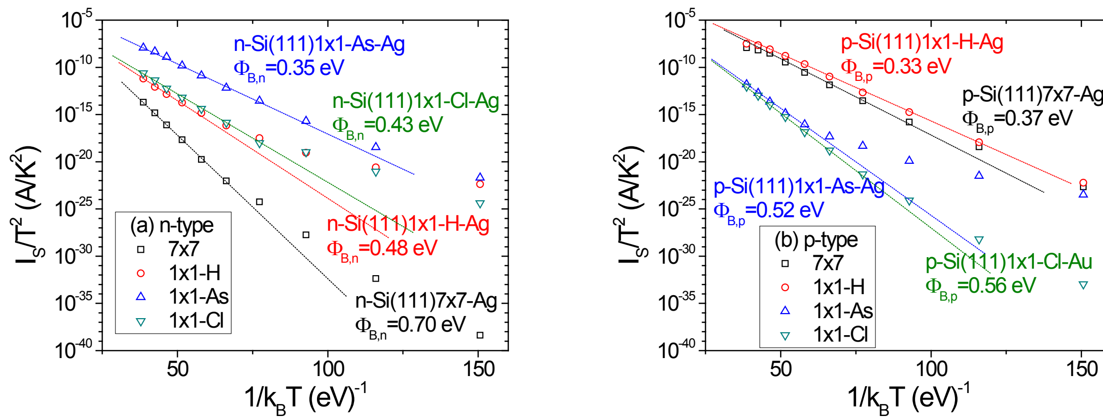

Figure 16. Richardson plots for the Schottky junctions of Ag on clean and various adsorbate-terminated Si(111) substrates, (a) n-type, (b) p-type.

be regarded as the dominant SBH at the lower temperature range, which is another indication of SBH inhomogeneity. While generally in good agreement with SBH obtained from single-temperature I-V measurements, activation energy analysis tended to render SBHs that were somewhat less, as shown in Table III. As pointed out [58], such a discrepancy is also indicative of inhomogeneity in the barrier height under study. One notes that this discrepancy is particularly large for SB on n-type H-Si(111) and is also quite significant for SB on n-type Si(111)-Cl.

Selected C-V plots are presented in Fig. 17. As shown in Table III, C-V measurements have reproduced the systematic trends observed by I-V and AE techniques, and have largely corroborated the magnitudes of the SBH's deduced from I-V measurements. For each specific interface, the SBH measured by the C-V technique is seen to exceed that measured by I-V measurement, frequently by an appreciable amount. The most straightforward explanation of such a difference between I-V and C-V measurements is the presence of non-uniformity in the

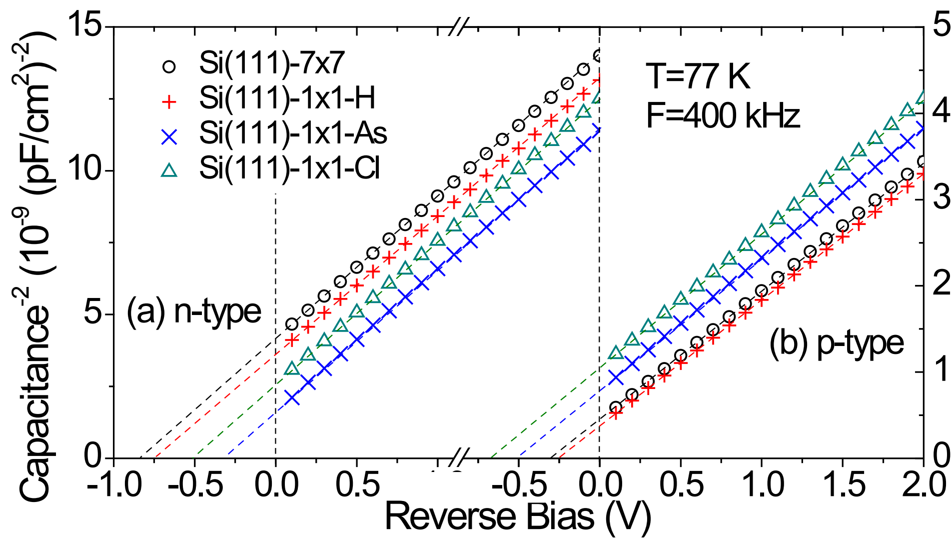

Figure 17. Experimental C-V characteristics for Schottky diodes formed on clean, H-, As- and Cl-terminated Si (111) surfaces, (a) n-type, (b) p-type.

Table III. SBH of Ag on adsobate-terminated Si(111).

SBH values were measured by I-V, C-V and Activation Energy (AE) techniques.

Ag		SBH (eV)			
		7×7	1×1-H	1×1-As	1×1-Cl
n-type	I-V	0.73±0.03	0.72±0.02	0.40±0.02	0.54±0.03
	AE	0.70±0.03	0.48±0.03	0.35±0.03	0.43±0.03
	C-V	0.86±0.06	0.80±0.03	0.46±0.02	0.64±0.04
p-type	I-V	0.35±0.02	0.32±0.02	0.60±0.02	0.61±0.02
	AE	0.37±0.03	0.33±0.03	0.52±0.03	0.56±0.03
	C-V	0.41±0.02	0.40±0.03	0.68±0.02	0.78±0.03

SBH. The constancy in the slopes of the C-V plots verified that the doping level of the substrate was unaffected by different surface treatments.

In addition to the proposed "partisan interlayer" mechanism, the SBH shift observed for the ATS has an alternative explanation that needs to be addressed. Being a shallow n-type dopant for Si, arsenic in-diffusion could lead to an apparent increase of the p-type SBH and a decrease in the n-type SBH [59, 60]. Simple calculations (see Appendix A) show that the magnitude of the SBH shift observed presently requires As diffusion to at least a depth of ~10 nm, whereas the diffusion length of As in Si for the actual UHV anneal, is estimated to be ~0.01 nm. This estimate, combined with the facts that Cl does not contribute to shallow impurity levels in Si safely rules out surface doping as relevant for the SBH change presently observed.

Presently, the SBH is demonstrated to be dramatically modified, in the prescribed direction, by changing the electron affinity of the starting semiconductor surface. Whenever the interaction between the metal and the ATS can largely be avoided, its n-type SBH should be given by Eq. (4). Plugging in the widely quoted electron affinity of clean Si (4.05 eV) and work

function of Ag (4.73 eV), the n-type SBH is predicted to be ~0.38 eV and -0.15 eV (ohmic), respectively, for the ideal As- and Cl- partisan interlayers. The excellent agreement for the As interlayer, which demonstrates the validity of the partisan interlayer approach, owes its success to the excellent chemical stability reported for the Si(111)1×1-As surface [38], and its likely preservation at the Ag interface. On the other hand, the decrease (0.2-0.3 eV) in n-type SBH observed for the Si(111)-Cl is much less than expected for idealized interlayers. While potential errors in the estimation of the electron affinity may be partly to blame, the interaction between Ag and the Cl-interlayer is more likely the main reason for this discrepancy. The ionicity of the Cl-Si bond makes it more susceptible to attacks by incidental charge, in the Ag beam or the environs. Thus it is reasonable to expect that the original 1×1-Cl structure is only partially intact at the interface with Ag, which would lead to a reduced amount of shift in the SBH and a pronounced inhomogeneity in its SBH, both of which were experimentally observed. The similarity in the SBHs measured for H-Si(111) and clean 7×7 is suggestive of the liberation of chemisorbed H from the interface. Interestingly, a low n-type SBH, 0.48 eV, was measured by AE for the Si(111)-H, indicative of an inhomogeneous interface with small, low-SBH regions. It should be pointed out that this particular observation is of the wrong sign for residual H-Si structure at the interface, but would be consistent with residual hydrogen at the interface that has become partisan to the Ag!

The present partisan interlayer approach is built on two sound principles: charge transfer in molecular chemistry and superposition of electrostatic potential, which are also the two cornerstones of a successful theory on SBH formation [2]. There is no fundamental limit on the kind of MS systems to which the partisan interlayer approach can be applied. There is, however, a requirement on the chemical stability of the ATS surface. One notes that it is usually not

difficult to design stable ATS for most semiconductors, if a decrease in the n-type SBH is desired, because ATS's terminated on large-electronegativity elements are expected to be resistant to oxidation. For some surfaces of a compound semiconductor, this may require two or more atomic layers of different chemical species to achieve a closed-shell electronic configuration with the desired surface dipole. A steeper challenge faces attempts to decrease the p-type SBH, which is a long-standing problem for some wide-gap ohmic contact technologies [61, 62], because a surface terminated with elements of low electronegativity usually offers poor resistance to oxidation and/or intermetallic reactions. One suggests that for such interfaces, an easier approach to weaken FL pinning, with a significant overall dipole in the intended direction, might be to also apply stable interlayer to the metal, for instance by using metallic nanoparticles capped with an interlayer that's partisan to the metal.

A significant modification of the SBH, without changing the metal, was demonstrated through the proposed partisan interlayer method. The increase in electron affinity of Si(111) surface, when terminated with electronegative Cl or As, was utilized to alter the MS interface dipole. The n-type SBH was found to decrease, and the p-type SBH increase, by as much as 0.40 eV, due to the interlayers.

CHAPTER 6. Schottky Barriers on S-Terminated Si(100): Ohmic Contact without Heavy Doping!

An important application of adjustability in SBH is the formation of low-resistance, ohmic contact, which is one where "the voltage drop across the contact is a negligibly small portion of the total applied voltage under normal working conditions" [63]. This can be accomplished by either having very low SBH for the junction, or by enhanced tunneling through the potential barrier with heavy doping [64, 65]. Presently, ohmic contact technologies rely largely on heavily-doped semiconductor to accommodate efficient conduction with negligible voltage drop. However, heavy doping may not be an available option to nano-scale devices or for some wide-bandgap semiconductors [66, 67], in which case low-contact-resistance solutions based on SBH adjustment have to be sought. Ordinarily when an ohmic junction is formed, the electronic transport is completely dominated by the series resistance in the circuit, without explicit information on how low the barrier height is, except that it is "low enough"; or how large the actual contact areas are, except that they are "large enough". In this work, the formation of ohmic contact was addressed along two different fronts. The partisan interlayer method on the Si(100) substrate was discovered to significantly reduce the Au SBH, to the state of ohmic contact [68]. Through the uses of special wafers and temperature-dependent measurement, the linear junction current was found to provide semi-quantitative information on the size and the distribution of SBH within these ohmic contacts. These discoveries could pave the way for the development of well-controlled ohmic contact technologies and for possible improvements in the characterization of ohmic contacts in general.

To study the partisan interlayer approach on tuning the SBHs by changing metals on one particular ATS surface, S-terminated Si(100) was chosen as the substrate, also because there are apparently conflicting reports of the SBHs on this surface in the literature. From the partisan interlayer mechanism, a lower n-type SBH (higher p-type SBH) than that for clean Si is expected on S-terminated Si surfaces. Such a shift would be largely in agreement with previous experiments on the segregation of S at silicide interfaces [69]. Reports of the opposing effect (a significant increase in the n-type SBH) due to sulfur can also be found [70, 71], although only from uncharacterized surfaces prepared *ex situ*. The resolution of this apparent conflict is of some importance, both from the perspective of understanding the formation mechanism of the SBH and for the purpose of practical applications. In the present work, SBHs on well-characterized Si(100)2×1 and Si(100)1×1-S surfaces, both formed under UHV conditions, were studied in detail. Ag, Au and In were all studies on these substrates for their widely varying work functions. For Au and In, SBH formed on atomically clean Si(100) has not been previously reported.

The Au-Si SBH system has a rich history of interesting dependencies. With its high work function, routinely processed Au has one of the highest SBH (>0.8 eV by CV) [72, 73] on n-type Si. However, the Au-Si SBH is known to exhibit an "aging" phenomenon [74-76] on cleaved Si surface. Also, Au-Si interfaces prepared in vacuum displayed no rectification until the diodes were exposed to ambient gas [77]. Diffusion of oxygen and water vapor was thought as the reason for the n-type SBH to increase by > 0.3 eV over a period that ranged from hours to months [78]. In other experiments, the formation of a Au-Si eutectic (silicide) phase at the interface was proposed [79, 80] and was thought to play a role in the time dependence of the Au SBH. While conclusive explanations of the minor mysteries described above are still missing,

suffice it to say however, that changes in the Au-Si interface microstructure could have a significant effect on its SBH. During the present experiments, non-uniform ohmic behavior was discovered for Au on n-type Si(100)1×1-S, the proper analysis of which necessitated the development of a special technique, from which quantitative information on not only the magnitude of the effective SBH but also the size of the dominant conducting areas could be extracted. This represents an improvement in the quantitative characterization of low-SBH contacts and will likely become a useful tool in the development of low-resistance contact technologies for lightly doped semiconductors.

The proposed technique uses the magnitude of the series resistance, which for inhomogeneous junctions depends, through its spreading-resistance component, on the lateral size of the dominant conducting path(s) at the interface. Once the average area for these dominant conducting patches is determined, the magnitude of the SBH is also known. To maximize the ratio of the spreading resistance to the total Si series resistance, the thickness of Si should be kept small. A thin Si layer also provides better spatial resolution as it eliminates the overlaps in conduction paths between neighboring patches. However, the thickness of Si cannot be too small as the spreading resistance needs to dominate parasitic resistances from other parts of the circuit. These considerations led to the selection of epitaxial Si wafers (epi-wafers), with a 5~10 μm lightly-doped (~10^{15} cm^{-3}) surface epi-layer grown on heavily doped Si(100) 6" wafers (n on n+ and p on p+) for the present study.

With respect to clean substrates, the work function of S-terminated Si(100) was found to consistently increase by ~0.13-0.15 eV, for both n- and p-type substrates, measured by Kelvin Probe (also see Table II in Chapter 4). It is noted that a larger increase was previously determined from photoemission measurements [41].

From I-V measurements, the overarching effect of S-termination was an increase in the n-type junction current and a decrease in the p-type junction current for any of the metals, by several orders of magnitude over that for the clean Si(100), as can be seen in Fig. 18, for example. These changes corresponded to shifts from the nominal SBH on clean Si, in excess of 0.1 eV in all cases, due to S-termination in the direction predicted by the proposed partisan interlayer mechanism. Table IV summarized the results from I-V, C-V, and activation energy measurements of Schottky diodes fabricated on both clean and S-terminated Si(100) surfaces with all three metals. Because of evidence, discussed below, for large scale SBH non-uniformity at some of the interfaces, the observed SBH and ideality factor from I-V measurements were

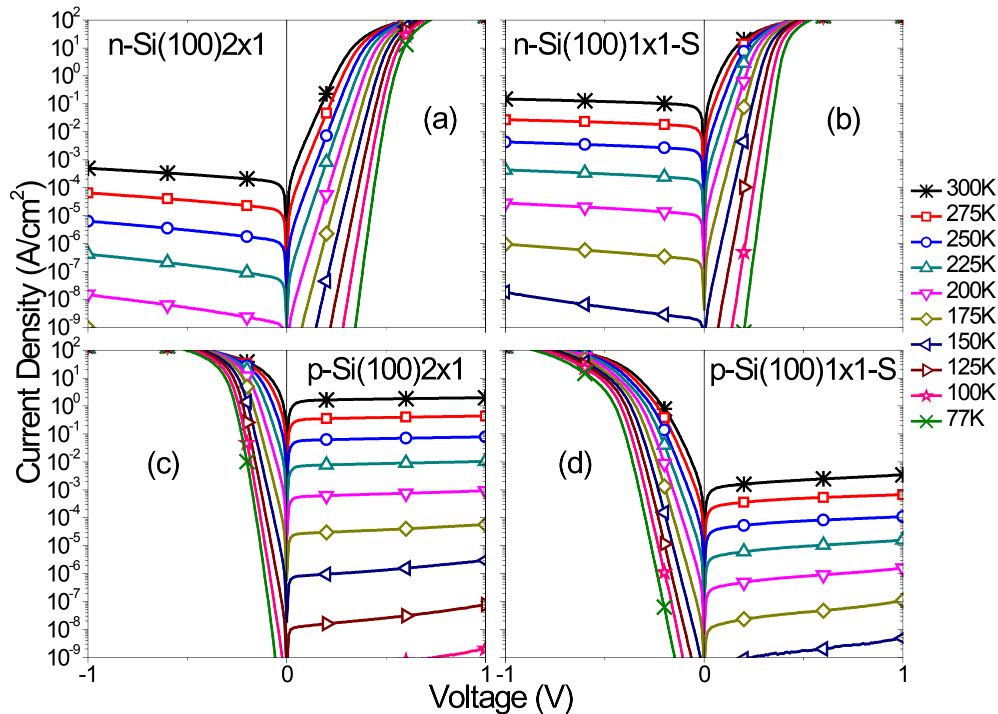

Figure 18. I-V characteristics at various temperatures for Ag Schottky barriers on Si(100).

Surface structure and doping type are specifically marked in each panel.

reported as a range in Table IV. Within each category, the very high-end of the SBHs and the low-end of the ideality factors were usually those observed at near room temperature, which were also the "nominal" values to be compared with values reported in the literature. The lower SBH deduced by fitting the lower temperature I-V traces should be regarded as an upper bound of the operating SBH at those temperatures because the actual area of the patch(es) giving rise to this current component was unknown, but expected to be much less than the entire diode area [58]. Examples of how the apparent SBH and ideality factor vary with the measurement temperature, as a result of SBH inhomogeneity, could be found in Figs. 18, 19 and 21.

All I-V traces from representative Ag diodes in Fig. 18 were essentially semi-logarithmic and apparently of high quality. Nevertheless, some level of inhomogeneity in the SBH was still suggested by the ideality factor (Table IV), which was more pronounced for samples shown in Figs. 18(a) & 18(d) than Figs. 18(b) & 18(c). Fig. 19 displays the forward current characteristics for Au on p-type substrates of clean and S-terminated Si(100), where ideality factors and SBHs

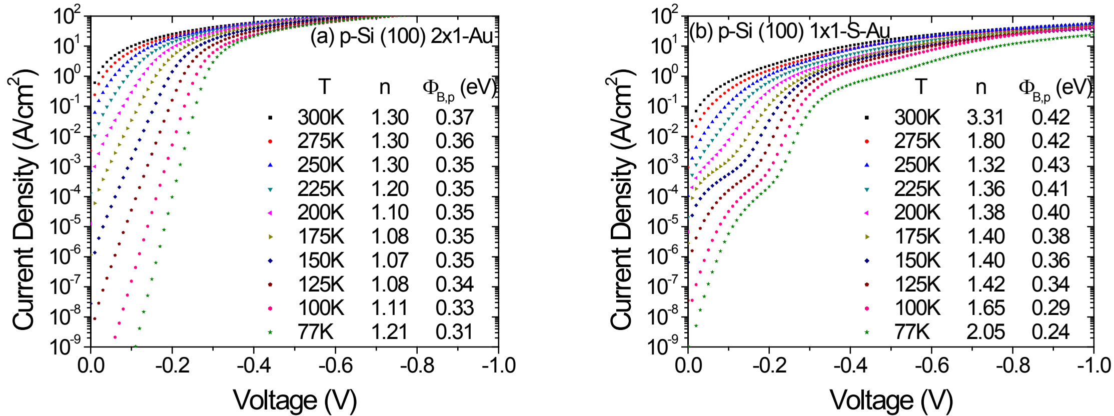

Figure 19. Representative I-V curves under forward bias from Schottky diodes of Au on (a) clean Si(100)2×1 and (b) S-terminated Si(100)1×1 surfaces, both p-type, showing ideality factors and SBH at each individual temperature.

obtained from fitting each individual curve into Eq. (8) are listed. The total currents at higher temperatures were dominated by series resistance, where ideality factors appeared to be larger than that at low temperatures. The listed SBH values calculated at individual temperatures clearly show the SBH variation, which is more significant at the p-Si(100)1×1-S-Au junction (Fig. 19(b)) than at the p-Si(100)2×1-Au junction (Fig. 19(a)). The S-terminated interface also shows a significant low-SBH patch at low-temperature curves.

The existence of inhomogeneity was also supported by the discrepancies in the SBH measured by different techniques for these junctions [58], summarized in Table IV. The present SBH results for Ag on clean Si(100)2×1, including the presence of SBH variations, were in good agreement with the findings of a prior UHV work [81]. Typical C-V characteristics of the Ag

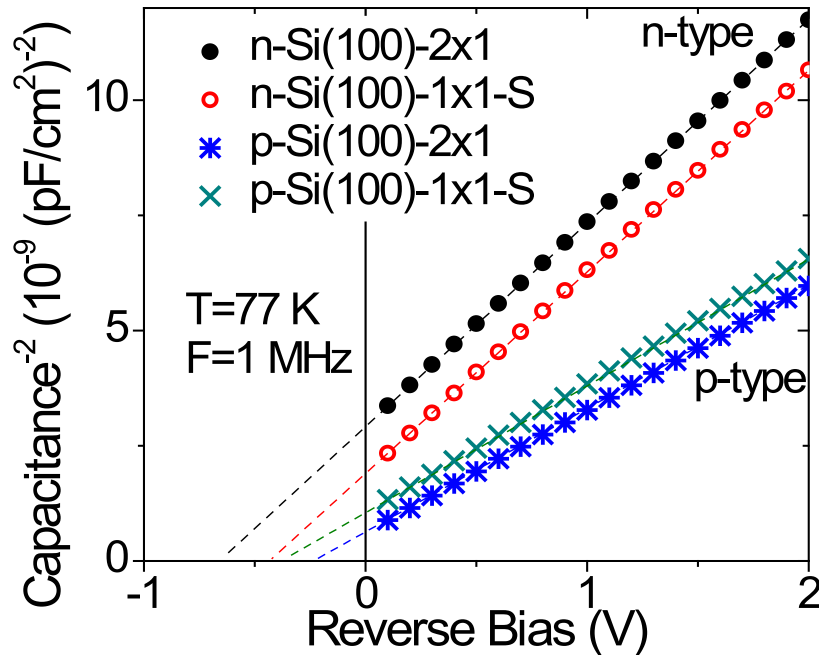

Figure 20. Experimental C-V characteristics for Schottky diodes of Ag formed on clean and S-terminated Si(100) surfaces.

diodes formed on different surface terminations and doping types were shown in Fig. 20. Capacitances were found to be frequency independent over wide frequency range and yield doping concentrations unaffected by the S-treatment and in agreement with the manufacturer-specified doping levels.

Richardson's plots of the saturation current, shown in Fig. 21, yielded straight sections at higher temperatures that were used for SBH determination, for all the Ag junctions. The lower-temperature end of the Richardson's plots tended to flatten and display a tangent with a considerably lower SBH than that characteristic of the rest of the curves. These lower values, which could be regarded as the dominant SBH at the lower temperature range, were also recorded in Table IV. Unlike single temperature I-V measurement, these lower-bounds

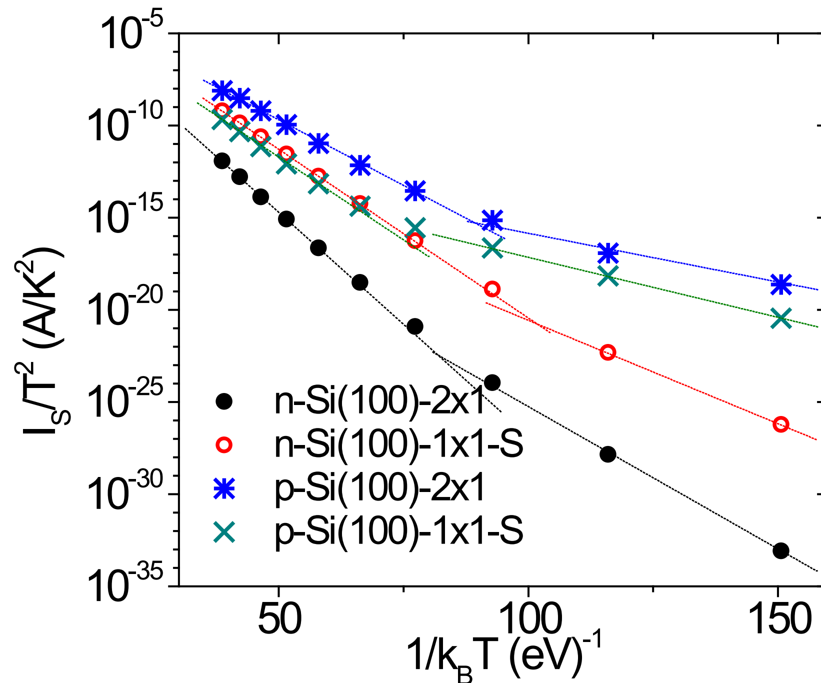

Figure 21. Richardson's plots of the saturation currents of Ag Schottky barriers formed on clean and S-terminated Si(100) surfaces.

Table IV. Summary of SBHs of In, Ag and Au on S-terminated Si(100) surfaces, measured by I-V (Φ_{I-V}), C-V (Φ_{C-V}), and activation energy (Φ_{AE}) techniques. I-V, AE results and ideality factors are presented as a range.

		In		Ag		Au	
		2×1	1×1-S	2×1	1×1-S	2×1	1×1-S
n-type	Φ_{I-V} (eV)	0.54~0.26	0.45~0.23	0.65~0.50	0.48~0.38	0.56~0.41	ohmic
	Ideality Factor	1.15~1.90	1.18~1.75	1.07~1.30	1.04~1.26	1.10~1.43	n/a
	Φ_{AE} (eV)	0.46~0.13	0.36~0.10	0.56~0.36	0.41~0.26	0.50~0.26	ohmic
	Φ_{C-V} (eV)	0.60±0.02	0.48±0.02	0.72±0.02	0.53±0.03	0.70±0.04	n/a
p-type	Φ_{I-V} (eV)	0.51~0.47	0.65~0.52	0.38~0.26	0.56~0.29	0.38~0.30	0.44~0.24
	Ideality Factor	1.11~1.70	1.04~1.33	1.04~1.30	1.11~1.95	1.07~1.21	1.32~2.05
	Φ_{AE} (eV)	0.47~0.12	0.62~0.35	0.33~0.11	0.42~0.15	0.34~0.23	0.40~0.12
	Φ_{C-V} (eV)	0.60±0.02	0.82±0.02	0.35±0.04	0.58±0.08	0.56±0.03	0.75±0.05

represented the real transport barrier from some dominant low-SBH patches, as the AE analysis was independent of the effective area of the current flow. Similar to the Ag results, the junction characteristics of In and Au Schottky barriers (not shown) also displayed varied degrees of SBH inhomogeneity at different types of interfaces. Nevertheless, a comparison of (the range of) the SBH observed on the clean Si(100)2×1 and the Si(100)1×1-S surfaces, for each individual metal, clearly established the expected effect on the SBH due to partisan interlayer mechanism with sulfur-termination. It was interesting that the SBH shift at the interface due to sulfur was typically on the order of 0.12-0.15 eV, similar to the measured WF shift in surface studies.

Perhaps the most unexpected among the present experimental results was the absence of a measurable SBH at the Au/n-Si(100)1×1-S junctions. The linearity of I-V traces, as shown in Fig. 22(a), over wide forward and reverse bias range, was repeatedly observed in different runs and was a distinguishing trait of "ohmic contact". The conventional definition of an ohmic contact is one where "the voltage drop across the contact is a negligibly small portion of the total

applied voltage under normal working conditions" [63], and is usually attributed to the presence of vanishing or very small SBH at the junction. The ohmicity of n-type Au-Si contact without heavy doping is ordinarily an unimaginable feat, because Au is one of the most extensively studied metallizations on Si and its SBH is widely recognized as one of the highest on n-type Si, ~0.8 eV [72, 73], when fabricated under non-UHV conditions. However, as Table IV revealed, the UHV-fabricated MS interfaces on clean Si(100)2×1 had a high level of SBH inhomogeneity. From AE results, the local FL position in the bandgap for Au was shown to span a range of ~0.66 eV, from ~0.26 eV (low-end of n-type SBH) below the conduction band minimum to ~0.20 eV (low-end of p-type SBH) above the valence band maximum, on clean Si(100)2×1. It was expected that on S-terminated surface, the Au SBH would remain significantly inhomogeneous and, because of the added negative dipole due to Si-S bonds, could conceivably reach very low SBH in certain locations to explain the observed ohmic behavior. Understanding how low the SBH was at the Au/n-Si(100)1×1-S interface was of great importance for the evaluation of the full effect of sulfur termination, although such an analysis seemed to have been made very difficult by the predominance of the series resistance in the I-V characteristics (Fig. 22(a)). Fortunately, as shown below, the epi-wafers chosen for the present work provided a rare opportunity to quantitatively answer not only questions on how low the SBH had to be for ohmic behavior to be observed but also, in cases of inhomogeneous junctions, the question of how large these low-SBH "hot spots" needed to be to produce the observed experimental results.

One noticed from Fig. 22(a) that, contrary to the behavior expected of Schottky barriers, the junction current increased as the temperature was decreased from room temperature, and only dropped for the lowest temperature (77K), where the current also displayed rectification. This variation in the effective "series resistance" deduced from the (forward) junction current was in

good agreement with the reported trend of the bulk resistivity of 2.1×10^{15} cm^{-3} n-doped Si, used in these studies: ρ_{300K} (2.64 Ω·cm) > ρ_{225K} (1.53 Ω·cm) > ρ_{77K} (0.77 Ω·cm) ~ ρ_{150K} (0.75 Ω·cm) [82], and was a clear indicator of the excellent quality of the back contact. However, the magnitude of the measured series resistance was typically >100 times larger than that calculated from the nominal diode area and the thickness of the Si epi-layer. This discrepancy was obviously a result of the inhomogeneous nature of the junction as the vast majority of current could be carried through a small portion of the interface. Current transport at inhomogeneous SBs was previously shown to depend not only on the magnitude of the spread in SBH

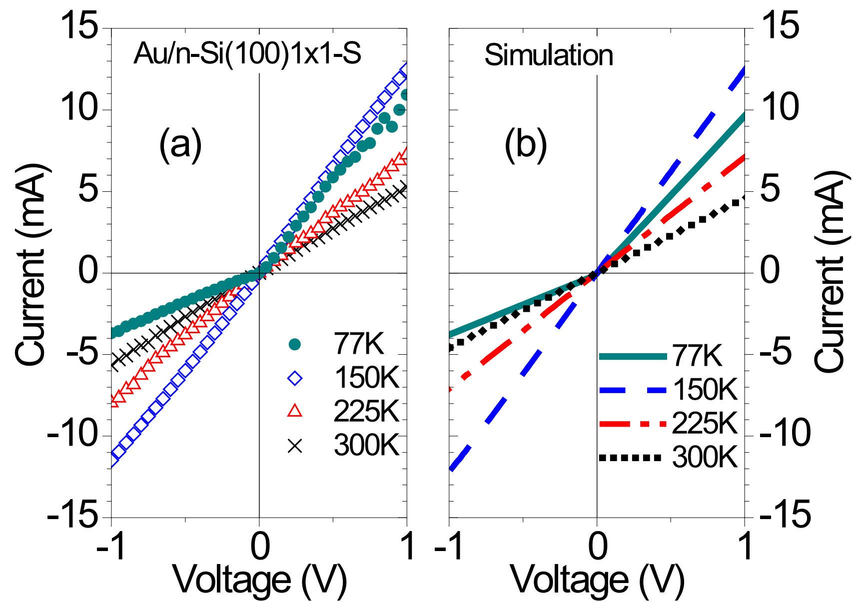

Figure 22. IV characteristics from experiment and numerical simulation.

(a) I-V characteristics from a typical Au/n-Si(100)1×1-S "diode" with an area of 7×10^{-4} cm^2;

(b) Simulated I-V characteristics from isolated low-SBH patches: 206 patches with SBH=0.032 eV and temperature-dependent area 4×10^{-10} cm^2 at T=300K; and 28 patches with SBH=0.015 eV and temperature-independent area 2×10^{-9} cm^2.

distribution, but also on the characteristic length with which the SBH varied [58]. On lightly doped semiconductors, potential “pinch-off” frequently took place, leading to bias-dependent “saddle-point” effective SBH for any patch, with an effective conduction area that was both bias- and temperature-dependent ($A_i \propto T$). However, to understand ohmic-type behavior at inhomogeneous contact, the bias dependence of the effective SBH (and area) could be ignored, because the actual voltage drop (electrochemical potential change) across the MS interface had to be an insignificant part of the applied bias, by virtue of ohmicity, and thus could not lead to significant changes in either the SBH or the area. Since it is anticipated that the transport takes place through small and dispersed low-SBH patches, the total junction current can be written as

$$I(V_a) = \sum_i I_i(V_a) = A^{**}T^2 \sum_i A_i \exp\frac{-\Phi_i}{k_B T}\left[\exp\frac{e\left(V_a - I_i R_i\right)}{k_B T} - 1\right], \qquad (10)$$

where V_a and A^{**} are the applied voltage and the Richardson constant, respectively. Φ_i, A_i, I_i, and R_i are, respectively, the SBH, the area, the current and the series resistance of the i-th conducting patch. An underlying assumption for Eq. (10) is that each patch independently contributes to the total current, i.e. the conduction paths from the hot spots do not significantly cross each other. This condition, which is essentially met if the patches are separated by more than L_{epi}, the thickness of the epi-layer (~5 μm), will be verified *a posteriori* in the analysis below. The series resistance associated with an independent patch, assumed circular in shape, has been found empirically to be [83]

$$R_i \approx \frac{\rho}{2\sqrt{A_i \pi}} \arctan\frac{2L_{epi}}{\sqrt{A_i/\pi}}. \qquad (11)$$

Note that the series resistance for a patch can vary from essentially uniform in nature ($= \rho L_{epi} / A_i$) when $\sqrt{A_i} >> L_{epi}$, to essentially spreading in nature ($= \rho \left(16 A_i / \pi\right)^{-1/2}$), as for a point contact, when $\sqrt{A_i} << L_{epi}$.

One first mentions a perhaps surprising fact that a vanishing barrier height ($\Phi_i = 0$), for even a uniform junction, is not a sufficient nor necessary condition for ohmic behavior. As seen from Eq. (10), what leads to a linearity in the junction current is the dominance of voltage drop across the series resistance, which in turn is due to the fact that the factor $\left|\exp\left\{\beta\left(V_a - I_i R_i\right)\right\} - 1\right|$ for the dominant current component(s) remained << 1 for the entire range of applied voltage. A prominent feature of Fig. 22(a) that underpinned the present quantitative analysis was that the current showed non-rectifying behavior at higher temperatures but rectifying, although still linear, behavior at the lowest temperature. This feature and extensive numerical simulations based on Eqs. (10) and (11) showed that the observed I-V characteristics, Fig. 22(a), could not have been caused by low-SBH patches with identical effective SBH. Rather, patches with effective SBH of >~0.03 eV and ones with effective SBH of <~0.03 eV needed to be both present to produce the experimental current. Additionally, the majority of the current from the latter group (<0.03 eV) needed to go through patches that were each at least ~2×10^{-11} cm^2 in size and had a total combined area equaling ~0.01%-0.8% of the actual diode area (see Appendix B). The number of patches per area was thus limited and amounted to an average separation between patches of >6.3 μm, justifying the use of Eq. (10). Furthermore, to closely reproduce the experimental I-V characteristics, it was discovered that the effective conduction areas for some of the low-SBH patches should be temperature-dependent, i.e. the patches should be pinched-off. From the temperature-dependence of bulk resistivity at the doping concentration currently

involved, it would be impossible for the currents at 77K and 150K to separate as Fig. 22(a) does, as shown in Fig. 23, where representative small patches that may possibly contribute to the ohmic behavior currently observed, with temperature dependent or independent areas. As illustrated in Fig. 22(b), the observed junction current from a particular sample, Fig. 22(a), could be essentially modeled by the co-existence of just two types of low-SBH patches. Because the junction current of a diode depends on the specific SBH distribution inside, the I-V characteristics of different diodes or different runs are expected to vary slightly. Temperature-dependent I-V characteristics from two other diodes are shown in Figs. 24(a) and 24(b). When

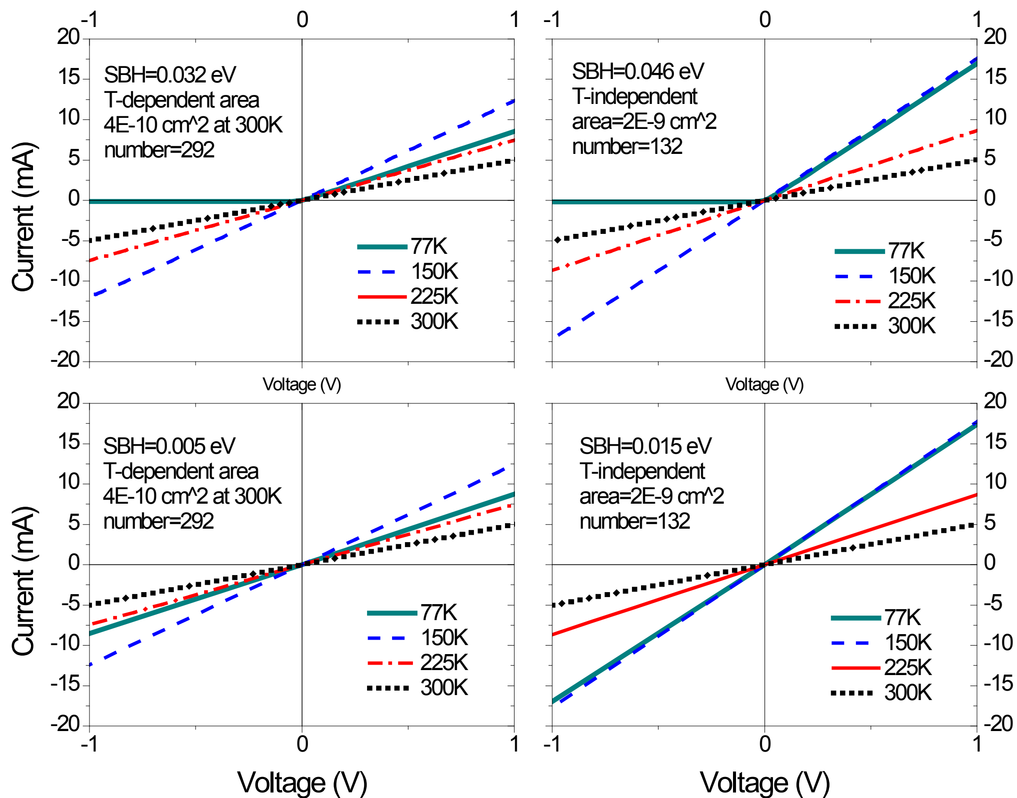

Figure 23. Possible components of small patches contributing to the ohmic behavior of n-type Si(100)1×1-S-Au.

plotted on the linear scale, the characteristics from different diodes may appear significantly different. However, as the figure caption reveals, the results of detailed analysis of the conduction patches in these diodes are similar. It could be concluded that the local SBH at certain small portions of the Au/n-Si(100)1×1-S interface was at least as low as ~0.03 eV. Even though the ohmic current was modeled without considering contribution due to tunneling, the present conclusions regarding the inhomogeneity in the effective barrier and the dimensions for the hot spots should remain valid regardless, because these conclusions were largely arrived at from the resistive behavior of the Si epi-layer. One also comments that the asymmetry in the current, clearly revealed in Eq. (10), has its roots in the matching condition of electronic states across a hetero-interface and, therefore, has validity beyond the thermionic emission theory.

Some degree of SBH non-uniformity is inevitable at all non-epitaxial MS junctions, since the SBH has been demonstrated to depend critically on the local structure of the MS interface [3, 58, 84-86]. For these interfaces, information on not only the average SBH, but also the extent of the inhomogeneity, is important for appropriate characterization of the SBH profile and understanding of the SBH mechanism. Through temperature-variable measurements, the present work studied the average SBH, as well as the range of its variation, for three different metals on atomically clean Si(100) and sulfur-terminated Si(100). Variable degrees of inhomogeneity were found for the SBH at all the interfaces studied in this work. The polarized S-Si bonds (surface negative, bulk positive) on the well-characterized surface of Si(100)1×1-S were observed to lead to an across-the-board shift in the SBH distribution, in the direction anticipated through the partisan interlayer mechanism and experimentally demonstrated for the Si(111) system [55]. This shift was ~0.1-0.2 eV for In and Ag on either type Si and for Au on p-type Si, consistent with the WF shift presently measured for the sulfur-terminated surface. The observation of ohmic

characteristics on n-type Si(100)1×1-S, which represents nominally a ~0.5 eV drop in SBH, was intriguing, considering that the increases in the p-type SBH and the EA were only 0.1-0.15 eV. However, as Table IV revealed, the UHV-fabricated Au-Si interface on clean Si(100)2×1 had a high level of SBH inhomogeneity. From AE results, the local FL position in the bandgap for Au was shown to span a range of ~0.63 eV, from ~0.26 eV (low-end of n-type SBH) below the conduction band minimum to ~0.23 eV (low-end of p-type SBH) above the valence band maximum, on clean Si(100)2×1. It was expected that on S-terminated surface, the Au SBH

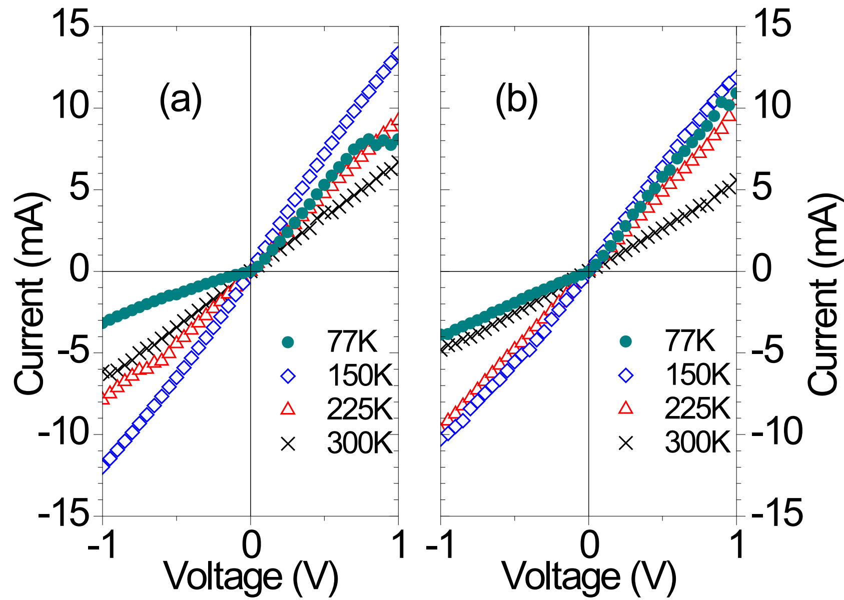

Figure 24. I-V characteristics from two additional diodes on the Au/n-Si(100)1×1-S samples.

Similar analysis as for Fig. 22 can closely reproduce these results with the following parameters: (a) 243 patches with SBH=0.032 eV and temperature-dependent area 4×10^{-10} cm^2 at T=300K, and 23 patches with SBH=0.015 eV and temperature-independent area 2×10^{-9} cm^2; (b) 185 patches with SBH=0.032 eV and temperature-dependent area 4×10^{-10} cm^2 at T=300K, and 31 patches with SBH=0.015 eV and temperature-independent area 2×10^{-9} cm^2.

would remain significantly inhomogeneous and, because of the added negative dipole, could conceivably reach very low SBH in certain locations to explain the observed ohmic behavior. Alternatively, in view of previous report of ohmic n-type Au-Si interface before air exposure [78], the presence of S in the present work could have stabilized certain Au-Si structure [87] at isolated locations, which gave rise to the very low SBH. All present interfaces were found to be stable, without observable change in electrical characteristics for over 6 months.

While the specific structure(s) responsible for the nearly vanishing SBH at Au/n-type Si(100)1×1-S interface could not be identified, the electrical profile of the dominant conduction regions was determined through the analysis technique introduced in this work. As demonstrated, the observed ohmic behavior was due to the presence of small patches with nearly vanishing local SBH. Previously, determination of the characteristics of isolated low-SBH patches was limited to non-ohmic junctions, through elaborate ballistic electron emission microscopy (BEEM) [88-90] involving ultrathin metal layers. The present analysis technique could greatly facilitate the development of contact technologies in other material systems, as it provides previously unavailable details on ohmic contacts. Although, it should be pointed out that this technique is only at its full power when a lightly-doped epi-layer of known thickness is used, as in the present study. Surprisingly and also excitingly, the patches presently giving rise to the ohmic current were shown to be at least as large as $\sim 2\times10^{-11}$ cm^2, which exceeded the nominal dimensions of the present-generation Si ULSI devices. This suggested that the structure(s) responsible for the low SBH possesses certain degree of stability to potentially be understood through high-resolution microscopy analyses and even be artificially synthesized through advanced nanofabrication techniques. This may have important ramifications for applications in Si and other nanoscale devices.

CHAPTER 7. Effect of Metal Interaction on the Schottky Barrier Height on the Adsorbate-Terminated Si Surfaces

To assess the effectiveness of the ATS candidates for partisan interlayer application, knowledge on the interaction between the ATSs with typical metal layers is required. In this chapter, we include additional experimental data, obtained with Au and In, with work functions of 5.1 eV and 4.12 eV [50], respectively, to complement the work already described for Ag (WF=4.26 eV) on Si(111). Specifically, it is to conclude the SBH results with three metals, In, Ag and Au, on the surfaces of Si(111)7×7, Si(111)1×1-As, Si(111)1×1-Cl, Si(100)2×1, and Si(100)1×1-S. Implications on the chemical stability of the ATSs that can be drawn from the entire body of available data are examined. A simple model on charge transfer and interface dipole is used as a guideline on the choice of materials in the partisan interlayer approach. In addition, the principles behind the partisan interlayer method and how they relate to existing theories on the formation of the SBH are briefly summarized. The extent of reaction between metals and the ATS surfaces employed for this study is inferred from electrical data compiled herewith and compared with available thermodynamic data.

Shown in different panels in Fig. 25 are temperature-dependent I-V characteristics obtained from Au junctions with both n-type and p-type clean Si(111)7×7 and Si(111)1×1-Cl. Even though most of the individual I-V curves were semi-logarithmic and apparently of high quality, the ideality factors were consistently found to exceed unity, suggesting the presence of a significant degree of SBH inhomogeneity in these diodes. The inhomogeneity of the SBH could also be concluded from the observed difference in the nominal SBHs obtained at individual temperatures, because low-SBH patches, if present, should increasingly dominate the junction

current as the temperature was lowered. The significant ranges in SBH deduced for the same diodes, from analysis of junction current at varied temperatures, were shown in Table V and provided only a lower bound to the full width of the actual SBH distributions at the interface, for lack of information on the actual areas of the low-SBH patches. Better quantitative estimates for the lower end of the SBH distribution were available through Richardson analysis of the junction current, where, as already pointed out, the range of activation-energies (slopes) observed for "curved" Richardson plots directly reflected distribution in the local SBH.

C-V characteristics of typical In and Au diodes fabricated on different surfaces were shown in Fig. 26. Capacitances were independent of frequency over a wide frequency range and

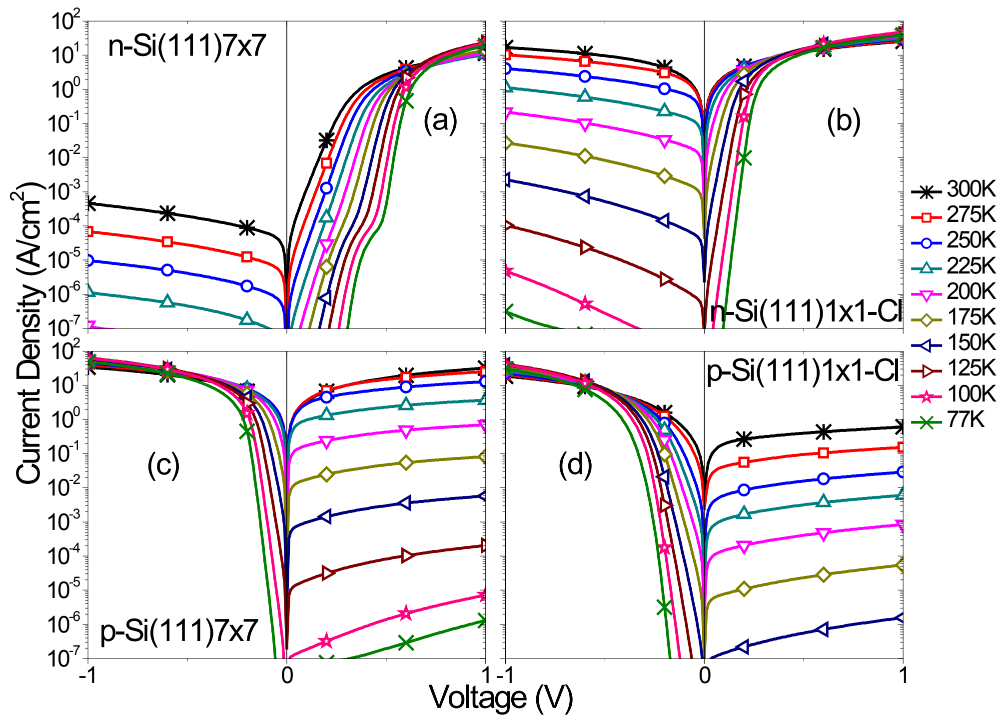

Figure 25. I-V characteristics at various temperatures for Au Schottky barriers on Si(111).

Surface structure and doping type are specifically marked in each panel.

yielded doping levels in agreement with the specified wafer doping levels. Being a measurement technique that was insensitive to the local variation of the SBH, C-V analysis deduced the "average" SBH for each interface. As summarized in Table V, the SBH for a particular interface depended on the measuring technique, which was another indicator of the overall non-uniformity SBH of all interfaces presently studied.

In addition to providing a range of variation in the magnitude of the SBH, the present body of experimental data also contained subtle information on the lateral length scale with which the SBH varied at the interface. For example, the unusual cross-over of the I-V traces for Au diodes at large forward bias, $I_{77K} > I_{300K}$ at V > ~ 0.5V (Fig. 25), could be traced the known

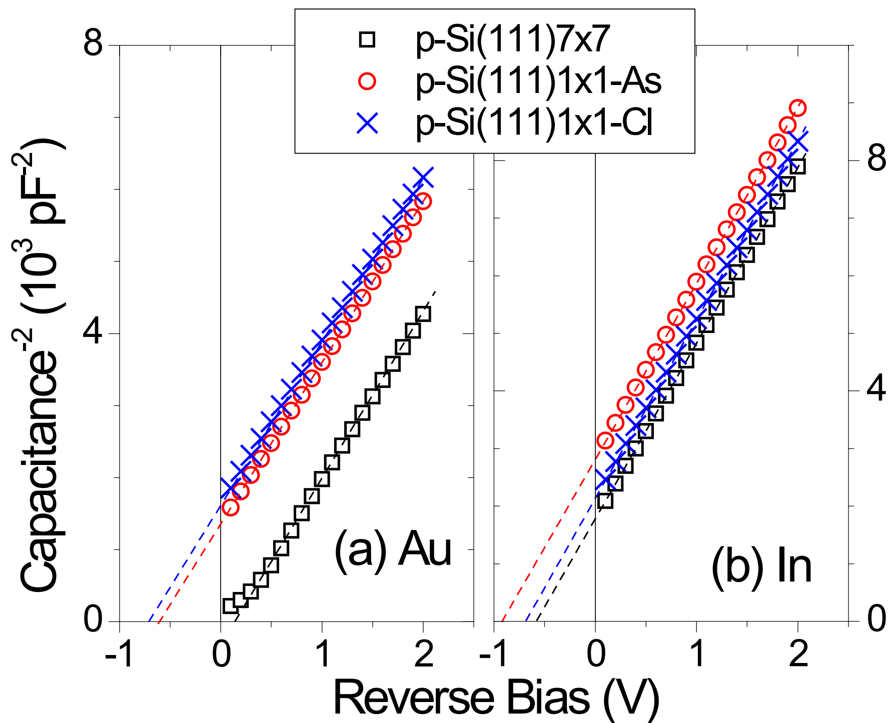

Figure 26. Representative C-V characteristics for Schottky diodes of (a) Au and (b) In formed on p-type clean, As and Cl-terminated Si(111) surfaces.

Table V. Summary of SBHs of In, Ag and Au on clean, As-, S- and Cl-terminated Si surfaces, measured by I-V ($\Phi_{I\text{-}V}$), C-V ($\Phi_{C\text{-}V}$), and activation energy (Φ_{AE}) techniques. I-V, AE results and ideality factors are presented as a range.

In		Si(111)			Si(100)	
		7×7	1×1-As	1×1-Cl	2×1	1×1-S
n-type	$\Phi_{I\text{-}V}$ (eV)	0.77~0.53	0.27~0.19	0.29~0.17	0.54~0.26	0.45~0.23
	Ideality Factor	1.03~1.39	1.12~1.42	1.75~2.95	1.15~1.90	1.18~1.75
	Φ_{AE} (eV)	0.80~0.30	0.17~0.15	0.12~0.10	0.46~0.13	0.36~0.10
	$\Phi_{C\text{-}V}$ (eV)	0.84±0.05	0.36±0.04	0.34±0.02	0.60±0.02	0.48±0.02
p-type	$\Phi_{I\text{-}V}$ (eV)	0.61~0.51	0.81~0.66	0.66~0.54	0.51~0.47	0.65~0.52
	Ideality Factor	1.03~1.25	1.23~1.47	1.04~1.24	1.11~1.70	1.04~1.33
	Φ_{AE} (eV)	0.60~0.44	0.73~0.62	0.61~0.45	0.47~0.12	0.62~0.35
	$\Phi_{C\text{-}V}$ (eV)	0.62±0.05	0.97±0.03	0.76±0.02	0.60±0.02	0.82±0.02
Ag		Si(111)			Si(100)	
		7×7	1×1-As	1×1-Cl	2×1	1×1-S
n-type	$\Phi_{I\text{-}V}$ (eV)	0.76~0.57	0.42~0.35	0.57~0.40	0.65~0.50	0.48~0.38
	Ideality Factor	1.10~1.51	1.07~1.40	1.08~1.77	1.07~1.30	1.04~1.26
	Φ_{AE} (eV)	0.70~0.42	0.35~0.22	0.43~0.25	0.56~0.36	0.41~0.26
	$\Phi_{C\text{-}V}$ (eV)	0.86±0.06	0.46±0.02	0.64±0.04	0.72±0.02	0.53±0.03
p-type	$\Phi_{I\text{-}V}$ (eV)	0.37~0.32	0.62~0.33	0.63~0.51	0.38~0.26	0.56~0.29
	Ideality Factor	1.05~1.25	1.08~2.10	1.15~1.40	1.04~1.30	1.11~1.95
	Φ_{AE} (eV)	0.37~0.30	0.52~0.16	0.56~0.33	0.33~0.11	0.42~0.15
	$\Phi_{C\text{-}V}$ (eV)	0.41±0.02	0.68±0.02	0.78±0.03	0.35±0.04	0.58±0.08
Au		Si(111)			Si(100)	
		7×7	1×1-As	1×1-Cl	2×1	1×1-S
n-type	$\Phi_{I\text{-}V}$ (eV)	0.68~0.42	0.64~0.37	0.39~0.26	0.56~0.41	ohmic
	Ideality Factor	1.17~1.83	1.15~1.46	1.18~1.40	1.10~1.43	n/a
	Φ_{AE} (eV)	0.48~0.23	0.38~0.21	0.29~0.16	0.50~0.26	ohmic
	$\Phi_{C\text{-}V}$ (eV)	0.95±0.02	0.86±0.02	0.50±0.03	0.70±0.04	n/a
p-type	$\Phi_{I\text{-}V}$ (eV)	0.31~0.23	0.39~0.26	0.43~0.33	0.38~0.30	0.44~0.24
	Ideality Factor	1.17~1.49	1.21~1.60	1.15~1.60	1.07~1.21	1.32~2.05
	Φ_{AE} (eV)	0.28~0.16	0.27~0.17	0.31~0.25	0.34~0.23	0.40~0.12
	$\Phi_{C\text{-}V}$ (eV)	0.20±0.04	0.68±0.02	0.80±0.03	0.56±0.03	0.75±0.05

temperature-dependence of bulk Si with specified doping levels, and was indicative of the excellent quality of the back ohmic contact(s). Under such well controlled experimental

conditions, the series resistance (R_S) for diodes of a fixed size should be independent of the metal used or the magnitude of the SBH, if the junction is uniform. However, the series resistances for Au diodes on n-type (or p-type) Si were found to be systematically larger, by ~ 20-100%, than those measured presently from Ag or In diodes. A reasonable explanation of this difference, which is more pronounced at lower temperatures, is that the lateral distribution of the current density at the Au interfaces was less uniform than other interfaces, and therefore suffered more from the "spreading" contribution to the series resistance. For this effect to be observed at all, the lateral length scale with which the SBH varied at the Au interface should be a noticeable fraction of the wafer thickness (500 μm). One therefore expects that, at lower temperatures, the majority of the current at the Au junction to come from small patches spatially separated by > 25 μm!

Even though the SBH was largely inhomogeneous for every MS interface presently studied, the choice of the ATS surface still exerted a prominent effect on the (average) magnitude of the SBH. From Figs. 25 and 26, the n-type (p-type) SBH for either In or Au was smaller (larger) on Cl- and As-terminated Si(111) than it was on clean Si(111)7×7, in agreement with the partisan interlayer mechanism. To systematically assess the effectiveness of the different ATSs within the PI approach, the "average" n-type SBH presently obtained by C-V measurement were summarized in Table VI, along with SBH values presented in previous chapters. Note that for the n-type SBH of the Au/Si(100)1×1-S interface, the value quoted was actually the Si band gap minus the measured p-type SBH. This replacement, necessitated by the presence of small ohmic patches at the n-type junction that prevented the C-V measurement, was well within the spirit and the intentions of Table VI. One first noticed, from Table VI, that the average SBHs for the three metals on the clean Si(111)7×7 were considerably higher than those on the clean Si(100)2×1. Although previously observed for Ag [81], this trend had not been

Table VI. Summary of C-V measured n-type SBHs of In, Ag, and Au on clean and ATS surfaces. (*The n-type Au/Si(100)1×1-S SBH value was the Si band gap minus p-type SBH.)

n-type SBH (eV)	In	Ag	Au
Si(111)7×7	0.84±0.05	0.86±0.06	0.95±0.02
Si(111)1×1-As	0.36±0.04	0.46±0.02	0.86±0.02
Si(111)1×1-Cl	0.34±0.02	0.64±0.04	0.50±0.03
Si(100)2×1	0.60±0.02	0.72±0.02	0.70±0.04
Si(100)1×1-S	0.48±0.02	0.53±0.03	0.37±0.05*

widely recognized or discussed, perhaps because only a handful of studies on the SBH of atomically clean Si surfaces was so far available. Such a dependence of the average SBH on wafer orientation and the significant degree of SBH inhomogeneity found at all the interfaces recently studied were generally at odds with the charge-neutrality-level concept advocated in many SBH theories [91-93]. One notes in passing that a similar, although weaker, dependence of the SBH on Si orientation was also observed in several non-UHV studies [89, 94]. The significant effect of the choice of the ATS on the average SBH, as summarized in Fig. 27, was present for all the metals, and for both Si(111) and Si(100). Fig. 27 was displayed in a format (n-type SBH against the metal work function) historically employed to deduce the FL-pinning strength and possibly to analyze the microscopic mechanism for SBH formation. However, since the SBHs were already known to be significantly inhomogeneous, and hence "unpinned", the same analysis would no longer serve such a purpose. Nevertheless, the shape of such a plot, albeit only of the averages of the SBH, could still be suggestive and characteristic of the nature of the overall MS interaction.

From Fig. 27, one noticed that, among all the ATS surfaces, the Si(111)1×1-As was the only one on which the SBH was observed to systematically increase with the metal WF. An interface behavior parameter (S-parameter, $S_\Phi = \partial\Phi_{Bn} / \partial\phi_M$) of ~ 0.53 could be deduced for the Si(111)1×1-As surface with a direct linear fit. This S-parameter was considerably larger than that usually found for Si (e.g. an S-parameter of ~ 0.1 could be deduced presently from the Si(111)7×7 data.), and was an indication that the FL at the Si(111)1×1-As interface was only "weakly pinned". In other words, the Si(111)1×1-As surface did not interact with deposited metal as strongly as the clean Si surface. The lack of strong metal-ATS interaction was a condition for the PI approach to succeed (Cf. Eq. 4), because SBH tuning could then be achieved

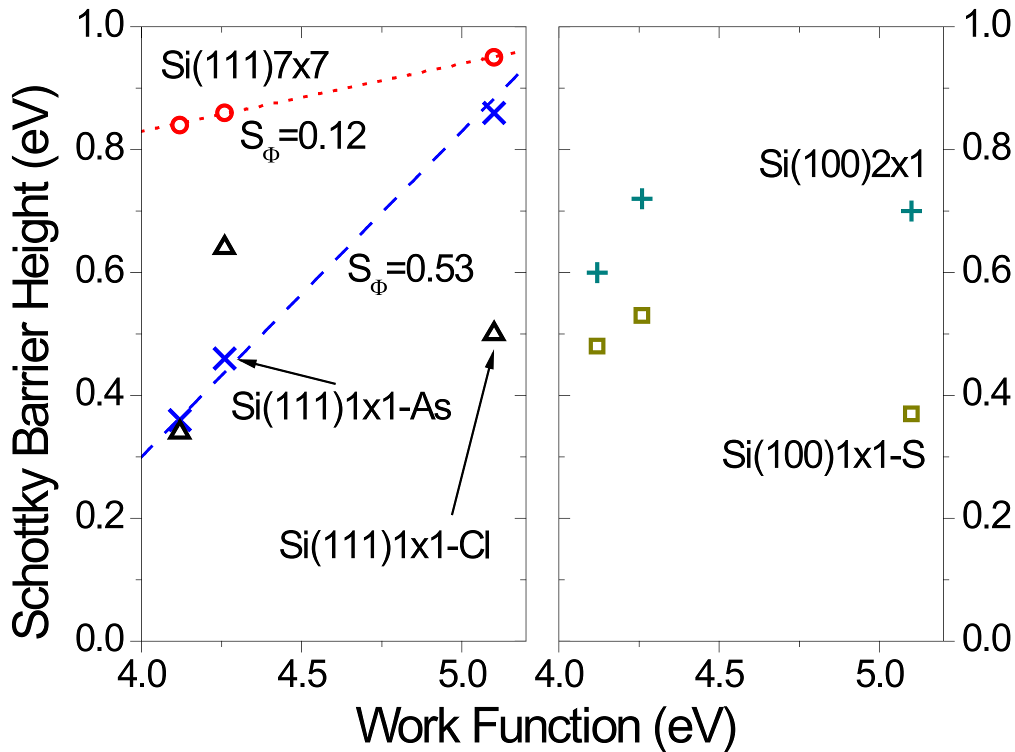

Figure 27. Dependence of n-type Schottky barrier heights on metal work function.

SBHs from Table V, against the polycrystalline values of the metal work function: In, 4.12 eV; Ag, 4.26 eV; and Au, 5.1 eV.

through the choice of metal work function. On the Si(111)1×1-Cl and Si(100)1×1-S surfaces, the dependence of the average SBH on the metal WF was more complex than predictable from the simple PI mechanism. There was a very sizeable decrease, ~ 0.22-0.48 eV, in the average SBH for any of the metals on Si(111)1×1-Cl, from that on clean Si(111). Such a decrease in SBH was in agreement with the increase in the electron affinity when Cl was used as surface termination. However, the measured average n-type SBH did not simply increase with the metal work function. Rather, the n-type SBH for Au, which had the largest WF among the metals, was found to be considerably lower than that for Ag. A similarly trend was observed for SBH measured on Si(100)1×1-S surface, in that the n-type SBH was lowered for all metal, but particularly dramatically for Au. In fact, portions of the Au/Si(100)1×1-S interface had extremely small n-type SBH such that the entire junctions behaved electrically as nearly perfect ohmic contact. These observations suggested that the interaction of some metals, Au in particular, with the Si(111)1×1-Cl and the Si(100)1×1-S surfaces could be significant and led to interface structures that were different from that envisioned in the partisan interlayer approach. Therefore, electrical characteristics alone seemed to suggest that the Si(111)1×1-As surface was more stable against metal interaction than the other two ATS surfaces. Previously, all three ATS surfaces were shown experimentally to be reasonably stable against air exposure. Theoretical calculations suggested that the Si(111)1×1-As, with a negative surface energy of ~5.34 eV per adsorbate atom [95] might be slightly more stable than either the Si(111)1×1-Cl (1.6 – 4.3 eV) [96] or the Si(100)1×1-S (5.2 eV) [97], although it should be pointed out that the methods used in these calculations were different. One noted that the stability of a real surface, in addition to being dependent on the energy of perfect surface structure, might ultimately depend on the densities of localized and extended defects. The significant inhomogeneity in the barrier height of these

junctions was in good agreement with the laterally inhomogeneous nature of interface interaction. As all three ATS surface presently studied could be categorized as having closed-shell electronic structures, the outermost orbitals were filled dangling bonds on the adsorbate atoms. These surface atoms thus more easily donated electrons than they could accept electrons. Therefore, it stood to some reason that the metal with the largest electronegativity, i.e. Au, seemed to have disrupted the ATS surface/interface the most. Of course, one should keep in mind that the systematic trends observed for the average SBH of the interfaces at best represented only a small fraction of the many different and inhomogeneous atomic processes that went on at the interfaces.

Presently, the SBH is demonstrated to be dramatically modified, in the intended direction, by changing the atomic structure and the electron affinity of the starting semiconductor surface. As discussed earlier, the success of such a "partisan interlayer" approach depends on the preservation of the interlayer structure at the interface and the absence of a strong chemical interaction between the metal and the interlayer. The methodology provides a general guideline on systematically tuning the SBH with reasonably expectable outcome. Results suggested that the As-Si(111) surface, among the three ATS surfaces presently studied, had the best stability against metal interaction and that Fermi level pinning was considerably weakened. This was therefore an excellent candidate for SBH tuning through the choice of the metal WF. The success of the present approach showed that the structure-dependent electrical dipole at the MS interface was the controlling factor for SBH and was the factor that needed to be modified in order to adjust the SBH.

CHAPTER 8. Summary

A systematic modification of the SBH was demonstrated through the proposed partisan interlayer method. SBH is shown to be dramatically tuned, in the intended direction, by changing the atomic structure and the electron affinity of the starting semiconductor surface. By using the atomic species with larger electronegativity than Si to form adsorbate-terminated Si surfaces, the electron affinities of these surfaces were reduced. Even though the SBH was largely inhomogeneous for every MS interface presently studied, the choice of the ATS surface still exerted a prominent effect on the (average) magnitude of the SBH. The n-type (p-type) SBHs on these ATS surfaces were decreased (increased) comparing to that on clean Si, with three different metals tested. In preliminary work also carried out in our laboratory, adsorbates with smaller electronegativity than that of Si, with their expected surface-positive dipole contributions, were shown to supply the opposite effect. Through the use of S-terminated Si(100) specialty substrate with thin lightly-doped epi-layer, nearly ideal ohmic behavior was obtained on Au, the metal with one of the highest SBH on Si. This feat would not have been accomplished without the thorough understanding of the Schottky barrier formation mechanism and the successful modeling of electron transport inhomogeneous MS interface. The effect of the SBH modification by partisan interlayer is predictable, simply from the electronegativity consideration and the chemical stability of the adsorbate-terminated surfaces against metal interaction. A systematic method to vary the SBH thus emerged and seemed viable for advanced applications.

APPENDIX

A. Camel Doping

Let the enriched surface doping level and depth be N_H and t_H, respectively, and the bulk doping level and the total depletion width be N_L and W, respectively. The actual doping level of the surface is $\left(N_H - N_L\right)$. The "offset" eV_{os} measured by C-V is $t_H^2 = \frac{2\varepsilon V_{os}}{eN_H}$, or $eV_{os} = \frac{e^2 t_H^2 N_H}{2\varepsilon}$. The variation of the band bending due only to the enriched doping is $V_{os}\left(1 - zt_H^{-1}\right)^2 + \text{const}$. The potential in the depletion region is approximately:

$$V\left(z\right) = V_{bb}\left(1 - \frac{z}{W}\right)^2 - V_{os}\left(1 - \frac{z}{t_H}\right)^2 + const$$

Let $\frac{\partial V}{\partial z} = 0$,

$$2V_{bb}\left(1 - \frac{z}{W}\right)\frac{1}{W} = 2V_{os}\left(1 - \frac{z}{t_H}\right)\frac{1}{t_H}$$

and we have $z_{peak} = \frac{N_H t_H - N_L W}{N_H - N_L}$

The difference between C-V and I-V measurements is

$$
\begin{aligned}
\Delta &= \Phi_{C-V} - \Phi_{I-V} = V_{bb} - V\left(z_{peak}\right) \\
&= V_{bb} - \left\{ V_{bb}\left(1 - \frac{N_H \frac{t_H}{W} - N_L}{N_H - N_L}\right)^2 - V_{os}\left(1 - \frac{N_H - N_L \frac{W}{t_H}}{N_H - N_L}\right)^2 \right\} \\
&= V_{bb} - \left\{ V_{bb}\left[\frac{N_H\left(1 - \frac{t_H}{W}\right)}{N_H - N_L}\right]^2 - V_{os}\left[\frac{N_L\left(\frac{W}{t_H} - 1\right)}{N_H - N_L}\right]^2 \right\} \\
&\approx V_{bb} - \left[V_{bb}\left(\frac{1 - \frac{t_H}{W}}{1 - \frac{N_L}{N_H}}\right)^2 - V_{os}\left(\frac{N_L W}{N_H t_H}\right)^2 \right] \\
&\approx V_{bb} - V_{bb}\left(\frac{1 - 2\frac{t_H}{W}}{1 - 2\frac{N_L}{N_H}}\right) + V_{os}\frac{N_L^2 \frac{2\varepsilon V_{bb}}{eN_L}}{N_H^2 \frac{2\varepsilon V_{os}}{eN_H}} \\
&\approx V_{bb} - V_{bb}\left(1 - 2\frac{t_H}{W}\right)\left(1 + 2\frac{N_L}{N_H}\right) + V_{os}\frac{N_L V_{bb}}{N_H V_{os}} \\
&= V_{bb}\left(2\frac{t_H}{W} - \frac{N_L}{N_H}\right).
\end{aligned}
$$

Here, the enriched surface doping level, N_H, is assumed to be the limit of the solid solubility of As in Si, ~10^{20} cm^{-3}, and the depletion width, W, is calculated with the bulk doping level N_L, ~10^{15} cm^{-3}. Therefore, the surface doping depth t_H is required to be at least 10 nm, for the observed $\Phi_{C-V} - \Phi_{I-V}$ to be 0.1 eV

B. Ohmic Analysis

Assume that the asymmetry in the junction current at 77K is due to a specific type of low-SBH patches. These patches must give essentially symmetric current at 150K over a bias range of $\pm 1.0V$. Assume that an isolated patch has an area of $A_{patch} = \pi R_{patch}^2$ and an SBH of Φ_{patch}.

$$I_0 = A^{**} T^2 A_{patch} \exp\{-\Phi_{patch} / k_B T\} = A_{patch} J_0$$

We define the assymetry condition at 77K as "at +1V bias, the current is roughly ten times that of current at -1V". Since we anticipate that the reverse current is roughly I_0, we look for conditions that will give us a forward current of $> 10 I_0$ at +1 V, which suggests that the spreading resistance must be

$$10 I_{0,77} \cdot R_{sp,77} \sim 1V,$$

$$A^{**} T^2 A_{patch} \exp\{-\Phi_{patch} / k_B T\} \times \frac{\rho}{2\sqrt{A_{patch} / \pi}} = 0.1V.$$

We have $J_{0,77} \ \rho_{77} \sqrt{A_{patch} \pi} \approx 0.2V$.

The other constraint is that the current is symmetric at 150K, which essentially suggests that a current of magnitude $\sim 5 J_{0,77}$ must be flowing at 150K with a reverse bias of less than 0.3 kT, say $\sim 0.2 k_B T = 30 \cdot k_B$. In other words,

$$5 J_{0,77} = 5 A^{**} 77^2 \exp\{-\Phi_{patch} / k_B 77\} < A^{**} 150^2 \exp\{-\Phi_{patch} / k_B 150\} \cdot 0.2$$

$$\exp\{\Phi_{patch} / 0.0066 - \Phi_{patch} / 0.0129\} = \exp\{\Phi_{patch} \cdot 74\} > \sim 6$$

$$\Phi_{patch} > 0.024 eV \, !$$

Plugging $\Phi_{patch} \sim 0.03 eV$ back into earlier equation, we get $J_{0,77} = 112 \cdot 77^2 \cdot 0.01 = 7 \times 10^3$ and, therefore, $A_{patch} \geq \left(\frac{0.2}{7000 * 1.2} \right)^2 \frac{1}{\pi} = 1.8 \times 10^{-10} cm^2$. These are not mesoscopic in size!

$$I_{0,77} = 1.3 \times 10^{-6} \, Amp$$

The perfectly ohmic component in the junction has a SBH such that

$$0.2 I_{0,77} \cdot R_{sp,77} \sim 1V$$

$$0.2 * 112 * 77^2 \exp\{-\Phi_{patch} / .0066\} A_{patch} \times \frac{\rho}{2\sqrt{A_{patch} / \pi}} > 1$$

Note that $A_{patch} \times \frac{\rho}{2\sqrt{A_{patch} / \pi}}$ cannot be greater than ρd_{epi}, where d_{epi} is the thickness of the epilayer. We have, therefore, for a single huge patch,

$$0.2 * 112 * 77^2 \exp\{-\Phi_{patch} / .0066\} 1.2 * 0.0005 \sim 1,$$

or $\Phi_{patch} < 0.029 eV$, and for very small patches,

$$0.2 * 112 * 77^2 \exp\{-\Phi_{patch} / .0066\} \sqrt{A_{patch} \pi} \rho / 2 \sim 1$$

$$0.2 * 112 * 77^2 \exp\{-\Phi_{patch} / .0066\} A_{patch} = 0.007 / N$$

$$A_{patch} = \pi \left(\frac{0.007\rho}{2N} \right)^2 \qquad D_{patch} = 0.007\rho / N$$

$$0.2 * 112 * 77^2 \exp\{-\Phi_{patch} / .0066\} = \frac{2N}{0.007\pi\rho^2} = 63N$$

$$\Phi_{patch} = 0.05 - .0066 \ln N$$

$$N < \sim 2000$$

It is only a slightly more restrictive constraint if the interface voltage drop is 0.1 kT rather than 0.2 kT.

For the case where the current is barely linear, N=2000, SBH=0, patch separation is 6.3 μm, and the patch diameter is $D_{patch} = 4.2 \times 10^{-6}\ cm$.

At 77K, the forward current is 15 A/cm^2 at +1V. Because the diode has an area of 8E-4 cm^2, the actual current is ~ 10 mA, of which 7 mA (70%) is the ohmic (symmetric) component. If all this current is from one big ohmic patch, this patch, with a SBH of 0.029 eV, will have a series resistance of 143 ohms, and an area of $1.2 * 0.0005 = 143 * A$ A=4.2E-6 cm^2. This is in the regime of essentially parallel conduction but with some spreading resistance contribution. If the one huge single patch has a SBH of 0 eV, it will have an area of $0.2 * 112 * 77^2 A_{patch} = 0.007$ $A_{patch} = 5 \times 10^{-8}$ cm^2.

REFERENCES

1. Brillson, L.J., *Surfaces and Interfaces of Electronic Materials*. 1st ed. 2010, Berlin: Wiley-VCH.
2. Tung, R.T., *Recent advances in Schottky barrier concepts.* Materials Science and Engineering: R: Reports, 2001. **35**(1-3): p. 1-138.
3. Tung, R.T., *Schottky-barrier formation at single-crystal metal-semiconductor interfaces.* Physical Review Letters, 1984. **52**(6): p. 461-464.
4. Heslinga, D.R., et al., *Atomic-structure-dependent Schottky barrier at epitaxial Pb/Si(111) interfaces.* Physical Review Letters, 1990. **64**(13): p. 1589-1592.
5. Wang, A. and W.A. Anderson, *Metal-semiconductor contacts to n-*$ZnS_{0.07}Se_{0.93}$. Journal of Electronic Materials, 1996. **25**(2): p. 201-205.
6. Hasegawa, F., et al., *Reduction of Schottky barrier heights by surface oxidation of GaAs and its influence on DLTS signals for the midgap level EL2.* Solid-State Electronics, 1988. **31**(2): p. 223-228.
7. Hattori, K. and Y. Torii, *A new method to fabricate Au/n-type InP Schottky contacts with an interfacial layer.* Solid-State Electronics, 1991. **34**(5): p. 527-531.
8. Coleman, J.J., *CONTROLLED BARRIER HEIGHT INP SCHOTTKY DIODES PREPARED BY SULFUR DIFFUSION.* Applied Physics Letters, 1977. **31**(4): p. 283-285.
9. Tung, R.T., *Chemical Bonding and Fermi Level Pinning at Metal-Semiconductor Interfaces.* Physical Review Letters, 2000. **84**(26): p. 6078.
10. Tung, R.T., *Formation of an electric dipole at metal-semiconductor interfaces.* Physical Review B, 2001. **64**(20): p. 205310.
11. Schottky, W., *Zur Halbleitertheorie der Sperrschicht- und Spitzengleichrichter.* Zeitschrift fur Physik, 1939. **113**(5-6): p. 367-414.
12. Mott, N.F., *The theory of crystal rectifiers.* Proceedings of the Royal Society of London Series a-Mathematical and Physical Sciences, 1939. **171**(A944): p. 0027-0038.
13. Schlüter, M., *Chemical trends in metal-semiconductor barrier heights.* Physical Review B, 1978. **17**(12): p. 5044-5047.
14. Mead, C.A. and W.G. Spitzer, *Fermi Level Position at Metal-Semiconductor Interfaces.* Physical Review, 1964. **134**(3A): p. A713.
15. Bardeen, J., *Surface States and Rectification at a Metal Semi-Conductor Contact.* Physical Review, 1947. **71**(10): p. 717.
16. Cowley, A.M. and S.M. Sze, *Surface States and Barrier Height of Metal-Semiconductor Systems.* Journal of Applied Physics, 1965. **36**(10): p. 3212-3220.
17. Tersoff, J., *Schottky barriers and semiconductor band structures.* Physical Review B, 1985. **32**(10): p. 6968.
18. Louie, S.G., J.R. Chelikowsky, and M.L. Cohen, *Ionicity and the theory of Schottky barriers.* Physical Review B, 1977. **15**(4): p. 2154.
19. Mönch, W., *Barrier heights of real Schottky contacts explained by metal-induced gap states and lateral inhomogeneities.* Journal of Vacuum Science & Technology B, 1999. **17**(4): p. 1867.
20. Spicer, W.E., et al., *Unified defect model and beyond.* Journal of Vacuum Science and Technology, 1980. **17**(5): p. 1019.

21. Hasegawa, H. and H. Ohno, *Unified disorder induced gap state model for insulator--semiconductor and metal--semiconductor interfaces.* Journal of Vacuum Science & Technology B: Microelectronics and Nanometer Structures, 1986. **4**(4): p. 1130.
22. Aboelfotoh, M.O., et al., *Schottky-barrier behavior of metals on n- and p-type 6H-SiC.* Physical Review B, 2003. **67**(7): p. 075312.
23. McKee, R.A., et al., *The interface phase and the Schottky barrier for a crystalline dielectric on silicon.* Science, 2003. **300**(5626): p. 1726-1730.
24. Campbell, I.H., et al., *Controlling Schottky energy barriers in organic electronic devices using self-assembled monolayers.* Physical Review B - Condensed Matter and Materials Physics, 1996. **54**(20): p. R14321-R14324.
25. Zuppiroli, L., et al., *Self-assembled monolayers as interfaces for organic opto-electronic devices.* European Physical Journal B, 1999. **11**(3): p. 505-512.
26. Selzer, Y. and D. Cahen, *Fine tuning of Au/SiO2/Si diodes by varying interfacial dipoles using molecular monolayers.* Advanced Materials, 2001. **13**(7): p. 508-511.
27. Hsu, J.W.P., et al., *Nature of electrical contacts in a metal-molecule-semiconductor system.* Journal of Vacuum Science and Technology B: Microelectronics and Nanometer Structures, 2003. **21**(4): p. 1928-1935.
28. Kampen, T., et al., *Barrier heights of organic modified Schottky contacts: Theory and experiment.* Applied Surface Science, 2004. **234**(1-4): p. 313-320.
29. Wang, W., T. Lee, and M.A. Reed, *Mechanism of electron conduction in self-assembled alkanethiol monolayer devices.* Physical Review B - Condensed Matter and Materials Physics, 2003. **68**(3): p. 354161-354167.
30. Lodha, S., P. Carpenter, and D.B. Janes, *Effect of contact properties on current transport in metal/molecule/GaAs devices.* Journal of Applied Physics, 2006. **99**(2): p. 1-9.
31. Vilan, A., A. Shanzer, and D. Cahen, *Molecular control over Au/GaAs diodes.* Nature, 2000. **404**(6774): p. 166-168.
32. Haick, H., et al., *Controlling semiconductor/metal junction barriers by incomplete, nonideal molecular monolayers.* Journal of the American Chemical Society, 2006. **128**(21): p. 6854-6869.
33. Kaxiras, E., *Semiconductor-surface restoration by valence-mending adsorbates: Application to Si(100):S and Si(100):Se.* Physical Review B, 1991. **43**(8): p. 6824-6827.
34. Olmstead, M.A., et al., *Arsenic overlayer on Si(111): Removal of surface reconstruction.* Physical Review B, 1986. **34**(8): p. 6041.
35. Headrick, R.L. and W.R. Graham, *Geometric structure of the Si(111): As-1×1 surface.* Physical Review B, 1988. **37**(2): p. 1051.
36. Copel, M., et al., *Atomic structure of the arsenic-saturated Si(111) surface.* Physical Review B, 1988. **37**(18): p. 10756.
37. Copel, M. and R.M. Tromp, *Structural perfection of the Si(111)-(1×1) As surface.* Physical Review B, 1988. **37**(5): p. 2766.
38. Uhrberg, R.I.G., et al., *Electronic structure, atomic structure, and the passivated nature of the arsenic-terminated Si(111) surface.* Physical Review B, 1987. **35**(8): p. 3945.
39. Becker, R.S., et al., *Geometric and Local Electronic Structure of Si(111)-As.* Physical Review Letters, 1988. **60**(2): p. 116.
40. Hybertsen, M.S. and S.G. Louie, *Theory of quasiparticle surface states in semiconductor surfaces.* Physical Review B, 1988. **38**(6): p. 4033.

41. Lacharme, J.P., N. Benazzi, and C.A. Sebenne, *Compositional and electronic properties of Si(001)2×1 upon diatomic sulfur interaction.* Surface Science, 1999. **433-435**: p. 415-419.
42. Rivillon, S., et al., *Gas phase chlorination of hydrogen-passivated silicon surfaces.* Applied Physics Letters, 2004. **85**: p. 2583.
43. Sakurai, S. and T. Nakayama, *Cl adsorption process on Si(1 1 1) surfaces.* Surface Science, 2001. **493**(1-3): p. 143-147.
44. Boland, J.J. and J.S. Villarrubia, *Formation of Si(111)-(1×1)Cl.* Physical Review B, 1990. **41**(14): p. 9865.
45. Eves, B.J. and G.P. Lopinski, *Formation and reactivity of high quality halogen terminated Si(1 1 1) surfaces.* Surface Science, 2005. **579**(2-3): p. L89.
46. Tung, R.T. and L. Kronik.
47. Kresse, G. and J. Furthmuller, *Efficient iterative schemes for ab initio total-energy calculations using a plane-wave basis set.* Physical Review B, 1996. **54**(16): p. 11169.
48. Kresse, G. and J. Hafner, *Ab initio molecular-dynamics simulation of the liquid-metal–amorphous-semiconductor transition in germanium.* Physical Review B, 1994. **49**(20): p. 14251.
49. Himpsel, F.J., G. Hollinger, and R.A. Pollak, *Determination of the Fermi-level pinning position at Si(111) surfaces.* Physical Review B, 1983. **28**(12): p. 7014.
50. Michaelson, H.B., *The work function of the elements and its periodicity.* Journal of Applied Physics, 1977. **48**(11): p. 4729-4733.
51. Ishizaka, A. and Y. Shiraki, *Low temperature surface cleaning of silicon and its application to silicon MBE.* Journal of the Electrochemical Society, 1986. **133**(4): p. 666-671.
52. Higashi, G.S., et al., *Ideal hydrogen termination of the Si (111) surface.* Applied Physics Letters, 1990. **56**(7): p. 656-658.
53. Kronik, L. and Y. Shapira, *Surface photovoltage phenomena: theory, experiment, and applications.* Surface Science Reports, 1999. **37**(1-5): p. 1-206.
54. Sommerhalter, C., et al., *High-sensitivity quantitative Kelvin probe microscopy by noncontact ultra-high-vacuum atomic force microscopy.* Applied Physics Letters, 1999. **75**(2): p. 286-288.
55. Li, Y., W. Long, and R.T. Tung, *Controlled modification of Schottky barrier height by partisan interlayer.* Solid State Communications, 2011. **151**(22): p. 1641-1644.
56. Baren, M., *The Ag-As (Silver-Arsenic) system.* Journal of Phase Equilibria, 1990. **11**(2): p. 113-116.
57. *Handbook of Chemistry and Physics*. 84 ed, ed. D.R. Lide. 2003, Boca Raton, FL: CRC Press.
58. Tung, R.T., *Electron transport at metal-semiconductor interfaces: General theory.* Physical Review B, 1992. **45**(23): p. 13509-13523.
59. Shannon, J.M., *Control of Schottky barrier height using highly doped surface layers.* Solid-State Electronics, 1976. **19**(6): p. 537-543.
60. Eglash, S.J., et al., *ENGINEERED SCHOTTKY-BARRIER DIODES FOR THE MODIFICATION AND CONTROL OF SCHOTTKY-BARRIER HEIGHTS.* Journal of Applied Physics, 1987. **61**(11): p. 5159-5169.
61. Ghosh, B., *Electrical contacts for II-VI semiconducting devices.* Microelectronic Engineering, 2009. **86**(11): p. 2187.

62. Liu, Q.Z. and S.S. Lau, *A review of the metal-GaN contact technology.* Solid-State Electronics, 1998. **42**(5): p. 677.
63. Scorzoni, A. and M. Finetti, *Metal/semiconductor contact resistivity and its determination from contact resistance measurements.* Materials Science Reports, 1988. **3**(2): p. 79-137.
64. Padovani, F.A. and R. Stratton, *Field and thermionic-field emission in Schottky barriers.* Solid-St. Electron., 1966. **9**: p. 695.
65. Crowell, C.R. and V.L. Rideout, *Normalized thermionic-field (T-F) emission in metal-semiconductor (Schottky) barriers.* Solid State Electronics, 1969. **12**(2): p. 89-105.
66. Liu, Q.Z. and S.S. Lau, *A review of the metal-GaN contact technology.* Solid-State Electronics, 1998. **42**(5): p. 677-691.
67. Pearton, S.J., et al., *Recent progress in processing and properties of ZnO.* Progress in Materials Science, 2005. **50**(3): p. 293-340.
68. Li, Y., W. Long, and R.T. Tung, *Inhomogeneous Ohmic Contacts: Barrier Height and Contact Area Determination.* Applied Physics Letters, 2012: p. accepted.
69. Zhao, Q.T., et al., *Tuning of NiSiSi Schottky barrier heights by sulfur segregation during Ni silicidation.* Applied Physics Letters, 2005. **86**(6): p. 062108.
70. Ali, M.Y. and M. Tao, *Effect of sulfur passivation of silicon (100) on Schottky barrier height: Surface states versus surface dipole.* Journal of Applied Physics, 2007. **101**(10): p. 103708.
71. Song, G., M.Y. Ali, and M. Tao, *A high Schottky barrier between Ni and S-passivated n-type Si(100) surface.* Solid-State Electronics, 2008. **52**(11): p. 1778-1781.
72. Kahng, D., *Conduction properties of the Au-n-type-Si Schottky barrier.* Solid State Electronics, 1963. **6**(3): p. 281-295.
73. van Otterloo, J.D., *Schottky barriers on clean-cleaved silicon.* Surface Science, 1981. **104**(2-3): p. L205-L209.
74. Turner, M.J. and E.H. Rhoderick, *Metal-silicon Schottky barriers.* Solid State Electronics, 1968. **11**(3): p. 291-300.
75. Mottram, J.D., et al., *Metal contacts to oxygen-contaminated silicon surfaces.* Journal of Physics D (Applied Physics), 1979. **12**(5): p. 773-786.
76. Varma, R.R., et al., *Interface states and the nature of metal-silicon contacts.* Journal of Physics D (Applied Physics), 1977. **10**(13): p. L171-L174.
77. Siffert, P., A. Coche, and G. Laustriat, *Rectifying Process in Surface Barrier Detectors.* IEEE Transactions on Nuclear Science, 1964. **11**(3): p. 244-248.
78. Ponpon, J.P. and P. Siffert, *Role of oxygen in the mechanism of formation of Schottky diodes.* Journal of Applied Physics, 1978. **49**(12): p. 6004-6011.
79. Nakashima, K., M. Iwami, and A. Hiraki, *Low temperature diffusion of Au into Si in the Si(substrate)-Au(film) system.* Thin Solid Films, 1975. **25**(2): p. 423-430.
80. Hiraki, A., *Low temperature reactions at Si/metal interfaces; What is going on at the interfaces?* Surface Science Reports, 1983. **3**(7): p. 357-412.
81. Weitering, H.H., et al., *Inhomogeneous Schottky barriers at Ag/Si(111) and Ag/Si(100) interfaces.* Journal of Applied Physics, 1996. **79**(10): p. 7820-7829.
82. Morin, F.J. and J.P. Maita, *Electrical properties of silicon containing arsenic and boron.* Physical Review, 1954. **96**(1): p. 28-35.
83. Cox, R.H. and H. Strack, *Ohmic contacts for GaAs devices.* Solid State Electronics, 1967. **10**(12): p. 1213-1218.

84. Palmstrom, C.J., et al., *Effect of orientation on the Schottky barrier height of thermodynamically stable epitaxial metal/GaAs structures.* Journal of Vacuum Science & Technology A, 1992. **10**: p. 1946-1953.
85. Dandrea, R.G. and C.B. Duke, *Interfacial atomic composition and Schottky barrier heights at the Al/GaAs(001) interface.* Journal of Vacuum Science & Technology B, 1993. **11**: p. 1553-1558.
86. Fujitani, H. and S. Asano, *Schottky-barrier height and electronic structure of the Si interface with metal silicides: $CoSi_2$, $NiSi_2$, and YSi_2.* Physical Review B, 1994. **50**(12): p. 8681-8698.
87. Narusawa, T., S. Komiya, and A. Hiraki, *Diffuse interface in Si (substrate)-Au (evaporated film) system.* Applied Physics Letters, 1973. **22**(8): p. 389-390.
88. Olbrich, A., et al., *Potential pinch-off effect in inhomogeneous Au/Co/$GaAs_{67}P_{33}$(100)-Schottky contacts.* Applied Physics Letters, 1997. **70**(19): p. 2559-2561.
89. Palm, H., M. Arbes, and M. Schulz, *Fluctuations of the Au-Si(100) Schottky barrier height.* Physical Review Letters, 1993. **71**(14): p. 2224-2227.
90. Haick, H., et al., *Controlling Au/n-GaAs junctions by partial molecular monolayers.* Physica Status Solidi (A) Applications and Materials Science, 2006. **203**(14): p. 3438-3451.
91. Tejedor, C., F. Flores, and E. Louis, *The metal-semiconductor interface: Si (111) and zincblende (110) junctions.* Journal of Physics C: Solid State Physics, 1977. **10**(12): p. 2163-2177.
92. Tersoff, J., *Schottky Barrier Heights and the Continuum of Gap States.* Physical Review Letters, 1984. **52**(6): p. 465-468.
93. Harrison, W.A. and J. Tersoff, *Tight-binding theory of heterojunction band lineups and interface dipoles.* Journal of Vacuum Science & Technology B: Microelectronics and Nanometer Structures, 1986. **4**(4): p. 1068-1073.
94. Palm, H., M. Arbes, and M. Schulz, *Nanometer-microscopy of the electron transmission through an ultrathin (3-22 nm) Au film and of the Au-Si schottky barrier height.* Applied Physics A Solids and Surfaces, 1993. **56**(1): p. 1-7.
95. Meade, R.D. and D. Vanderbilt, *Origins of stress on elemental and chemisorbed semiconductor surfaces.* Physical Review Letters, 1989. **63**(13): p. 1404-1407.
96. Ong, C.K. and L.P. Tay, *Chemisorption of fluorine and chlorine on a Si(111) surface.* Journal of Physics: Condensed Matter, 1989. **1**(6): p. 1071-1076.
97. Kruger, P. and J. Pollmann, *Ab initio calculations of Si, As, S, Se, and Cl adsorption on Si(001) surfaces.* Physical Review B, 1993. **47**(4): p. 1898.